Angiotensin II elicits robust calcium oscillations coordinated within juxtaglomerular cell clusters to suppress renin secretion.

Hiroki Yamaguchi[1], Nick A. Guagliardo[2*], Jason P. Smith[1], Fang Xu[1], Manako Yamaguchi[1], Lucas F, Almeida[1], Daisuke Matsuoka[1], Silvia Medrano[1], R. Ariel Gomez[1*], and Maria Luisa S. Sequeira-Lopez[1*].

[1]Department of Pediatrics, Child Health Research Center, University of Virginia School of Medicine, Charlottesville, Virginia.

[2]Department of Pharmacology, University of Virginia School of Medicine, Charlottesville, Virginia.

***Correspondence to:**

Maria Luisa S. Sequeira-Lopez,

409 Lane Road, Rooms 2001, 2006, and 2010, Charlottesville, VA 22908

Email: MSL7U@virginia.edu, Phone: 434-924-5065, Fax: 434-924-8936

and

R. Ariel Gomez,

409 Lane Road, Rooms 2001, 2006, and 2010, Charlottesville, VA 22908

Email: RG@virginia.edu, Phone: 434-806-8135, Fax: 434-924-8936

and

Nick A. Guagliardo,

1340 Jefferson Park Ave, Pinn Hall Rm 5045, Charlottesville, VA 22908

Email: nag4g@virginia.edu, Phone: 434-989-5531

Abstract

BACKGROUND: Juxtaglomerular (JG) cells are sensors that control blood pressure and fluid-electrolyte homeostasis. In response to a decrease in perfusion pressure or changes in the composition and/or volume of the extracellular fluid, JG cells release renin, which initiates an enzymatic cascade that culminates in the production of angiotensin II (Ang II), a potent vasoconstrictor that restores blood pressure and fluid homeostasis. In turn, Ang II exerts a negative feedback on renin release, thus preventing excess circulating renin and the development of hypertension. How Ang II suppresses renin release from JG cells remains elusive. Ang II may inhibit renin release via increased systemic pressure sensed by JG cells, or through a direct effect on Ang II receptors in JG cells, which in turn mediate intracellular calcium (Ca^{2+}) mobilization, a known suppressor of renin release. However, the intricate cellular events mediating Ca^{2+}-induced renin inhibition by Ang II are not fully understood. Further, the unique structural organization of the juxtaglomerular apparatus (JGA), with JG cells clustered around afferent arterioles, suggests complex intercellular interactions, potentially facilitating coordinated Ca^{2+} activity in response to Ang II. Here, we investigate the cellular processes that control Ca^{2+} mobilization and the signaling mechanisms elicited when JG cells are stimulated with Ang II within the intact anatomical context of the JGA. By examining these processes, we aim to elucidate the role of cellular organization in Ca^{2+}-mediated signaling and its impact on renin regulation within the JGA.

OBJECTIVE: To define intra- and inter-cellular Ca^{2+} dynamics, identify the driving ion channels, and elucidate their functional role in Ang II-stimulated JG cells within the native kidney structure.

METHODS AND RESULTS: We generated mice expressing JG cell-specific GCaMP6f, a genetically encoded Ca^{2+} indicator, under the *Ren1*^{c} promoter. *Ex vivo* Ca^{2+} imaging in acutely prepared kidney slices revealed that JG cells within clusters exhibit coordinated, robust Ca^{2+}

oscillations in response to Ang II stimulation, contrary to previous observations in isolated cells. These oscillations showed dose-dependent increases in occurrence and correlated with suppressed renin secretion. Pharmacological inhibition identified key drivers of these oscillations: endoplasmic reticulum Ca^{2+} storage and release, extracellular Ca^{2+} uptake via ORAI channels, and intercellular communication through gap junctions. Blocking ORAI channels and gap junctions alleviated Ang II inhibition of renin secretion.

CONCLUSION: In intact kidney slices, Ang II elicits synchronized Ca^{2+} oscillations in JG cells, driven by endoplasmic reticulum-derived Ca^{2+} release, ORAI channels, and gap junctions, leading to suppressed renin secretion.

Key Words

renin, blood pressure, kidney slices, renin-angiotensin system, calcium, ion channel, negative feedback loop, juxtaglomerular apparatus.

Renin, the rate-limiting enzyme of the renin-angiotensin system (RAS), plays a crucial role in blood pressure regulation and fluid-electrolyte homeostasis. Synthesized and secreted by juxtaglomerular (JG) cells, renin initiates a cascade that ultimately leads to the production of angiotensin II (Ang II). JG cells are strategically located as clusters of 5–7 cells at the tips of the afferent arterioles entering the glomeruli[1], forming an integral part of the juxtaglomerular apparatus (JGA). The JGA, composed of JG cells, the afferent and efferent arterioles, the extraglomerular mesangium, and the macula densa[2,3], provides a unique microenvironment for intricate cellular communication. Further, each JG cell is innervated by sympathetic nerve fibers[4], providing additional regulatory input. This complex anatomical arrangement allows JG cells to act as sensitive detectors of minute changes in perfusion pressure and to respond to signals from the surrounding structures, including the macula densa cells. The coordinated interactions within the JGA ensure that renin release is tightly regulated in response to the status of the extracellular fluid and blood pressure levels.

Intracellular calcium (Ca^{2+}) is a key regulator of renin synthesis and secretion[5–7] in JG cells, exhibiting a paradoxical relationship where elevated Ca^{2+} levels suppress renin production and release, contrary to most other secretory cells where Ca^{2+} stimulates hormone production (e.g., β- and α-cells of the pancreatic islets[8] or zona-glomerulosa cells of adrenal[9]). This inverse relationship governs both acute and chronic JG cell states. Ca^{2+} suppresses renin synthesis and secretion in JG cells by inhibiting adenylyl cyclase, which in turn leads to a reduction of cyclic adenosine monophosphate (cAMP), a potent stimulator of renin[6,10]. In addition, elevated Ca^{2+} may induce -through as yet unidentified mechanisms- chromatin folding at the renin gene locus, preventing binding of key transcription factors and the actions of key regulatory histone acetyltransferases[11–14], resulting in a loss of JG cell identity. Despite its crucial importance in

renin regulation, how intracellular Ca^{2+} dynamics in JG cells inhibit renin release remains poorly understood.

Renin is the rate-limiting enzyme responsible for the initial step of Ang II formation, the primary effector of the RAS that acts to increase blood pressure and extracellular fluid volume[15]. In turn, Ang II is thought to inhibit renin production in JG cells, although direct *in vivo* evidence of this negative feedback loop is lacking[16]. *In vitro* studies of primary cell cultures of renin-expressing cells demonstrated Ang II directly inhibits renin secretion through short-loop negative feedback[17,18], via intracellular Ca^{2+} signaling. Ang II has been shown to induce intracellular Ca^{2+} oscillations in isolated mouse JG cells, as demonstrated by simultaneous patch-clamp and fura-2 measurements[19]. However, these findings are limited by the absence of the complex cellular interactions present in the native kidney structure. JG cells are highly dependent on their surrounding tissue environment for proper function and identity maintenance, receiving constant physiological signals from adjacent cells, including other JG cells, vascular muscle cells (VSMCs), endothelial cells (ECs), macula-densa, and extraglomerular mesangium through gap junctions that facilitate cell-to-cell passage of signaling molecules and inorganic ions[20,21], components that are absent in isolated cells. The importance of this cellular and structural organization is underscored by the fact that JG cells isolated from kidney tissue cease synthesizing renin within 72 hours and differentiate into VSMCs[11,22], indicating their dependence on adjacent structures to sustain proper physiological function and identity[3].

This study aims to elucidate the intra- and inter-cellular Ca^{2+} dynamics in JG cells in response to Ang II stimulation within their native structural context. We utilize *ex vivo* Ca^{2+} imaging of acutely prepared kidney slices from transgenic mice expressing a JG cell-specific genetically encoded Ca^{2+} indicator, GCaMP6, to investigate the intra- and inter-cellular Ang II-elicited Ca^{2+}

responses in JG cell clusters and identify the ion channels and cellular interactions driving renin suppression in a physiologically relevant model. This approach will provide critical insights into JG cell function under normal and pathophysiological conditions, advancing our understanding of renal physiology and potentially informing new therapeutic strategies for hypertension and related disorders.

Results

Ang II evokes periodic Ca^{2+} signals within the JG cell cluster.

To study the intra- and inter-cellular Ca^{2+} dynamics in JG cells, we crossed *Ren1*$^{c+/Cre}$ mice, where Cre expression is driven by the *Ren1*^{c} promoter[11,23,24], with floxed-*GCaMP6f* mice[25], generating mice with JG cell-specific GCaMP6f expression (*Ren1*^{c}-*GCaMP6f* mice; Figure 1A). *Ren1*^{c}-*GCaMP6f* mice showed no overt renal phenotype, as evidenced by their unaltered body and kidney weight, kidney vascular development, plasma renin levels, *Ren1* mRNA expression, and carotid arterial blood pressure (Supplementary Figure 1). First, we confirmed JG cell-specific GCaMP6f expression in *Ren1*^{c}-*GCaMP6f* mice by immunofluorescence labeling of renin in the kidney cortex and assessed colocalization with GCaMP6f. Renin-positive cells colocalized with GCaMP6f expression in cells located in the JGA but not other renin lineage cells, including VSMC and mesangial cells (Figure 1B, Supplementary Figure 2). To measure acute changes in intracellular Ca^{2+} elicited by Ang II in JG cells, *ex vivo* kidney slices (75 μm thick) were prepared from *Ren1*^{c}-*GCaMP6f* mice, preincubated with 3 nM Ang II for ~20 min, and GCaMP6 fluorescence imaged with water-dipping objective lens under continuous perfusion of PIPES buffer (Figure 1C). In the absence of Ang II, JG cells were quiescent, with minimal Ca^{2+} activity. In contrast, 3 nM Ang II elicited robust Ca^{2+} oscillations (Ca^{2+} spikes; Figure 1D and Supplementary Movie 1). Further, changes in fluorescence propagated through the cytoplasm (Ca^{2+} wave) and oscillated successively between adjacent JG cells (Figure 1E). As indicated by kymograph plots, designated reslice lines tracked oscillatory Ca^{2+} waves within distinct JG cells and the sequential Ca^{2+} activity between adjacent cells, suggesting cell-cell interaction among the JG cell cluster members (Figure 1F). Collectively, our *ex vivo* imaging of acutely prepared kidney slices from *Ren1*^{c}-*GCaMP6f* mice

enabled us to study spatial-temporal Ca^{2+} dynamics in JG cells and reveal that Ang II elicits robust Ca^{2+} oscillations within the JG cell cluster.

Ang II-elicits Ca^{2+} spike bursts that correlate with renin secretion.

Next, we characterized the structure and dose-dependency of the Ca^{2+} activity elicited by Ang II in JG cells. To quantify the Ca^{2+} dynamics in distinct JG cells, we used the imaging analysis platform Mesmerize[26] and CaImAn[27] toolset for motion correction, unbiased region of interest (ROIs) detection, and signal demixing/extraction (Figure 2A) of each time series. The mean demixed fluorescent intensity for each ROI was plotted over time, and Ca^{2+} spikes were identified using custom Matlab software. This approach enabled us to quantitatively determine the number of Ca^{2+} spikes elicited by Ang II in distinct JG cells within the JG cell cluster. In kidney slices treated with one of four Ang II concentrations (50 pM, 300 pM, 3 nM, and 300 nM) for 25 minutes, JG cells demonstrated a dose-dependent increase in the number of Ca^{2+} spikes elicited by Ang II (Figure 2B). Further, Ca^{2+} spikes predominantly occurred within a burst of Ca^{2+} activity, with burst separated by quiescent periods (inter-burst interval) (Figure 2C).

To characterize the effect of Ang II on Ca^{2+} bursting properties, we quantified Ca^{2+} bursts in JG cells as previously described[9]. Briefly, we generated histograms of all ROI inter-spike intervals (periods) for each dose of Ang II with a Gaussian and an exponential function, defining the intersection of these functions as the threshold interval for determining intra- or inter-burst spike groupings (Supplementary Figure 3). Bursts were defined as three or more consecutive spikes with inter-spike periods shorter than the threshold (Event periods), while spike intervals exceeding the threshold indicate inter-burst periods of inactivity (Quiescent periods, Figure 2C, 2D). Spike

periods had a normal distribution with a distinct peak around 2.0–2.5 seconds (Figure 2D) with no differences in mean event periods across the Ang II concentrations (Figure 2E) in JG cell clusters. Notably, the mean number of bursts/min within a JG cell cluster was Ang II concentration-dependent (Figure 2F), with a maximal number of bursts elicited by 3 nM Ang II. Conversely, the mean duration of bursts within a slice (Figure 2G) and the mean number of Ca^{2+} spikes within a burst (Figure 2H) remained invariant across doses of Ang II. Furthermore, renin secretion in kidney slices treated with equivalent Ang II concentrations mirrored the dose-dependency between Ang II concentration and renin suppression predicted by the number of Ca^{2+} bursts (Figure 2I). Thus, in aggregate, our data indicate that the primary dose-dependent action of Ang II is to increase the incidence of stereotypic Ca^{2+} bursts, with consistent duration and a number of spikes per burst, that correlate with Ang II-inhibition of renin secretion.

Ang II-elicited Ca^{2+}-oscillations and renin secretion in JG cells are dependent on extracellular Ca^{2+}, primarily through ORAI channels.

Next, we asked if the Ang II-elicited Ca^{2+} spikes require Ca^{2+} from extracellular sources. Perfusion of 3 nM Ang II with the Ca^{2+} chelator ethyl-glycol tetraacetic acid (EGTA) in a "Ca^{2+}-free" buffer (0.1 mM Ca^{2+}) nearly eliminated Ca^{2+} oscillations (96.33% decrease). Restoring Ca^{2+} in the perfusion buffer (Recovery) induced renewed Ca^{2+} activity, indicating extracellular Ca^{2+} is necessary for Ca^{2+} oscillations in JG cells (Figure 3A, 3B). Ca^{2+} spikes were abolished 3–5 minutes after perfusion of Ca^{2+}-free buffer; this slow time course suggests extracellular Ca^{2+} may be necessary for response maintenance, rather than initiating acute calcium oscillations. To confirm changes in Ca^{2+} activity in Ca^{2+}-free buffer parallel functional changes in renin secretion, we measured renin from kidney slices in response to Ang II with and without extracellular Ca^{2+}.

Kidney slices treated with 3 nM Ang II for 30 min markedly decreased renin secretion in the presence of 2 mM Ca^{2+} but failed to elicit a change in renin in the Ca^{2+}-free condition (Figure 3C). These data are in agreement with the paradoxical response of JG cells, which display an inverse correlation between intracellular Ca^{2+} concentration and renin secretion[6]. In summary, our *ex vivo* Ca^{2+} imaging analysis and renin secretion assay highlight the function of Ang II in JG cells as an inducer of robust oscillatory Ca^{2+} signals and renin inhibition that is dependent on extracellular Ca^{2+} within the native structure of the kidney.

We next investigated cell membrane Ca^{2+}conductances responsible for maintaining Ang II-elicited Ca^{2+}-oscillations in JG cells. To identify candidate Ca^{2+} channels, we analyzed the gene expression profiles of major cytoplasmic Ca^{2+} permeable channels using single-cell RNA-seq data of *FoxD1*$^{+}$ descendants cells (*FoxD1*$^{+}$ cells are precursors for renin cells) isolated from *FoxD1*$^{cre/+}$*; R26R-mTmG* mice kidney at postnatal day 30, as previously reported[28] (Figure 3D). This analysis revealed the high expression of the following genes in the late JG cluster: $Ca_v1.2$ (*Cacna1c*), $Ca_v1.3$ (*Cacna1d*), $Ca_v3.1$ (*Cacna1g*), and $Ca_v3.2$ (*Cacna1h*) among L-type and T-type voltage-dependent Ca^{2+} channels (VDCC) α_1-subunits; TRPC1, TRPC3, TRPC4, TRPC6, and TRPV2 among canonical transient receptor potential (TRPC) and vanilloid TRP (TRPV) channels, which have been reported to be functionally expressed in JG cells[29–31]; and ORAI1 and ORAI3, which form a pore-forming subunit to mediate store-operated Ca^{2+} channels (SOCC) in combination with Ca^{2+}-sensing stromal interaction molecule (STIM) proteins[32,33]. Based on these findings, we conducted a screening of candidate Ca^{2+} conductances using pharmacological channel inhibitors and imaging GCaMP6 in JG cells in kidney slices from *Ren1*^{c}*-GCaMP6f* mice (Figure 3E). For each drug, JG cell clusters were imaged for 10 minutes with 3 nM Ang II perfusion (baseline), followed by the addition of channel inhibitors for 25 min (treatment), and mean Ca^{2+} spikes/minute

in the last 5 minutes of baseline and treatment conditions compared (Figure 3F). Application of 3 nM Ang II maintained consistent Ca^{2+} activity throughout 25-minute imaging experiments (Figure 3G); prolonged exposure to 488 nm fluorescence alone did not significantly influence the Ca^{2+} response to Ang II.

L-type and T-type VDCCs. L-type and T-type VDCC play crucial roles in generating and maintaining Ca^{2+} oscillations in various cell types, including neurons and endocrine cells. L-type VDCC exhibits high conductance with slow inactivation upon membrane depolarization[34] and is reported to be functionally expressed in isolated JG cells[35], while T-type channels are low conductance Ca^{2+} channels activated by small membrane depolarizations and are rapidly inactivated[36]. Dihydropyridine nifedipine[37] (a potent Cav1 antagonist) moderately decreased Ang II-elicited Ca^{2+} spikes (35.3% decrease) and TTA-P2[38] (a pan Cav3 family antagonist) did so partially (20.38% decrease), yet neither fully eliminated the Ca^{2+} spikes. (Figure 3H).

TRP channels. Based on the reports that the TRPC-mediated pathway inhibits renin release from JG cells[29], we targeted TRPC1/4/5 and TRPC3/6/7 subfamilies, which form non-selective, Ca^{2+}-permeable hetero-multimeric cation channels[39] with Pico145[40] and SAR7334[41], respectively. In addition, we used ruthenium red (RuR), a pan TRPV inhibitor[42], to target TRPV2 as well as TRPV4, which was suggested to be functional in JG cells as a mechanosensitive channel[30]. Inhibition with Pico145, SAR7334, or RuR did not reduce the number of Ang II-elicited Ca^{2+} spikes (Figure 3I; 28.48% decrease, 4.43% decrease, and 10.85% increase, respectively; not significant).

ORAI channels. To assess the contribution of ORAI channels to JG cell Ca^{2+} oscillation, we pharmacologically blocked both ORAI1 and ORAI3. Treatment with 50 μM trivalent lanthanide gadolinium (Gd^{3+}), a potent inhibitor of all ORAI isoforms (ORAI1, ORAI2, and ORAI3)[43–45],

drastically inhibited the number of Ca^{2+} spikes (92.16% decrease, Figure 3J) elicited by Ang II. In addition, a renin secretion from the kidney slices demonstrated that Gd^{3+} prevents the inhibition of renin secretion in 30 minutes under 3 nM Ang II but not in the absence of Ang II (Figure 3K). Since Gd^{3+} is also reported to affect other cell membrane cation channels[46], we applied used more selective ORAI inhibitors: low concentrations of Gd^{3+} (5 µM), which functions as an inhibitor of all ORAI isoforms[43–45] with greater selectivity, and pyrazole derivatives GSK-7975A, which inhibits recombinant ORAI1 and ORAI3 currents[47]. Both 50 µM Gd^{3+} and GSK-7975A significantly suppressed the number of Ca^{2+} spikes induced by 3 nM Ang II (5 µM Gd^{3+}; 63.72% decrease, GSK-7975A; 67.36% decrease, Figure 3L). Furthermore, GSK-7975A significantly attenuated the inhibition of renin secretion in kidney slices stimulated with 3 nM Ang II, but not in the absence of Ang II (Figure 3M).

Combined, these data indicate that ORAI channels strongly contribute to maintaining Ang II-elicited Ca^{2+}-oscillations and concomitant suppression of renin, while individual VDCC and TRPC1/4/5 channels only partially account for Ca^{2+} activity in JG cells.

Dependence of Ang II-elicited Ca^{2+} spikes on endoplasmic reticulum Ca^{2+} storage in JG cells.

Classically, oscillatory intracellular Ca^{2+} signals are generated through rapid Ca^{2+} release from the ER[48]. We investigated the dependence of ER Ca^{2+} and its release on Ang II-elicited Ca^{2+} oscillations in JG cells. Our single-cell RNA-seq data revealed high expression of (Sarco-) endoplasmic reticulum Ca^{2+}-ATPase (SERCA, *Atp2a*) and inositol 1,4,5-trisphosphate (IP3)

receptor (IP3R, *Ip3r*) genes in the JG clusters, while gene expression of ryanodine receptors (RyR, *Ryr*) was low (Figure 4A).

We first examined the SERCA, which transports cytosolic Ca^{2+} into the ER lumen, thereby controlling the amount of Ca^{2+} in the ER (Figure 4B). If Ang II-elicited Ca^{2+}-oscillation depended on ER stores and releases, blocking Ca^{2+} store filling would be expected to prevent Ca^{2+} spike generation. Indeed, the pharmacological blocking of SERCA with CPA[49] drastically inhibited the number of Ca^{2+} spikes (93.66% decrease, Figure 4C). Of note, simultaneously with the decrease in Ca^{2+} spikes, CPA induced a persistent and global increase in fluorescent intensity (Figure 4D), indicating elevated intracellular Ca^{2+}. This phenomenon represents a typical effect of Store-operated Ca^{2+} entry (SOCE) triggered by the depletion of ER Ca^{2+} stores[50], which has been reported in isolated JG cells as well[5,6].

To examine the dependence of ER release channels in JG cells, we blocked IP3R with a cell-permeable IP3R inhibitor, 2-Aminoethoxydiphenyl borate (2-APB)[51], and RyR with the RyR1 and RyR3 inhibitor Dantrolene[52] (Figure 4B). Treatment with 2-APB markedly decreased the Ca^{2+} spikes (93.79% decrease), while dantrolene did not affect the number of Ca^{2+} spikes (9.06% increase, Figure 4C). Ruthenium red, which also acts as a RyR inhibitor[53], further supports the non-contribution of RyRs to Ang II-elicited Ca^{2+}-oscillations in JG cells. In contrast to SERCA blockade, IP3R inhibition by 2-APB significantly decreased overall fluorescent intensity while simultaneously decreasing Ca^{2+} spikes (Figure 4E, 4F), which is likely due to 2-APB's effect as aSOCE inhibitor[54]. Taken together, these data indicate the dependence of Ca^{2+} storages and release from the ER via SERCA and IP3R on Ang II-elicited Ca^{2+}-oscillations in JG cells.

JG cell clusters require gap junctions to induce robust Ang II-elicited Ca^{2+} oscillations and coordinate to suppress renin secretion.

Through our *ex vivo* Ca^{2+} imaging approach, we observed that the Ca^{2+} signal propagates through the cytoplasm (Ca^{2+} wave) and oscillates successively between adjacent JG cells (Figure 1E, 1F), suggesting cell-cell interactions among the JG cell cluster members. In agreement with previous data demonstrating gap junctions are abundantly and functionally expressed in JG cells[20,21,55–57], our single-cell RNA-seq data showed a diverse and highly expressed gene expression profile of gap junction protein (e.g., Cx37, Cx40, Cx43, and Cx45) in JG cells and their adjacent cells, including VSMCs and ECs (Figure 5A). Thus, to broadly investigate the contribution of gap junctions to Ca^{2+} activity in JG cells with their neighboring cells, we applied a pan gap junction inhibitor, carbenoxolone (CBX)[58], and analyzed the Ca^{2+} signal pattern within the JG cell clusters. Notably, CBX effectively prevented Ang II-induced Ca^{2+} propagation across adjacent JG cells within the clusters (Figure 5B, Supplementary Movie 2) while markedly reducing the number of Ca^{2+} spikes (94.18% decrease, Figure 5C). Finally, we confirmed that CBX alleviated renin secretion inhibition within 30 minutes with 3 nM Ang II but not in the absence of Ang II (Figure 5D). These data support the requirement for gap junctions to facilitate Ang II-induced Ca^{2+} oscillatory activity within JG cell clusters, thereby suppressing renin secretion.

Discussion

Cells fluctuate in their cytoplasmic Ca^{2+} concentration to regulate versatile cellular processes — gene transcription, secretion, muscle contraction, development, etc.— and display diverse spatiotemporal Ca^{2+} dynamics[59,60]. In JG cells, cytoplasmic Ca^{2+} signals are crucial to suppress renin synthesis and secretion[5–7]. Ca^{2+} signals are activated by various physiological stimuli and hormones, including the octapeptide Ang II. In the intact kidney, JG cells receive constant signals from nearby cells, including other JG cells, macula-densa cells, VSMCs, ECs, extraglomerular mesangial cells, and sympathetic nerve terminals. In turn, those cells are interconnected by gap junctions that facilitate cell-cell communication via intracellular passage of secondary messengers and inorganic ions[20,21]. However, understanding the Ca^{2+} dynamics of JG cells in a setting that preserves the original kidney tissue structure, location of cells, and interconnection with their neighboring cells and their surrounding has not been explored. To overcome this limitation, here we use *ex vivo* tissue slices to visualize and define the signals and channels that drive the complex intracellular movements of Ca^{2+} upon exposure to Ang II, the natural end product of the RAS cascade and inhibitor of renin release. We show here that Ang II dosed-dependently induces robust and sustained bursts of Ca^{2+}-oscillations within each native JG cell and suppresses renin secretion. These Ca^{2+} bursts are mediated by intracellular Ca^{2+} release from the ER and maintained through influx of Ca^{2+} through ORAI channels. Further, inter-cellular gap junctions propagate coordinated Ca^{2+} signaling, serving as a critical modulator of renin inhibition by Ang II (Figure 6). Overall, these results highlight the complex molecular and cellular processes that govern the Ca^{2+} signaling responsible for the understudied and poorly understood negative feedback inhibition of renin synthesis and secretion.

Previous research demonstrated that Ang II induces oscillatory patterns of intracellular Ca^{2+} signals in isolated mouse kidney cells[19]. However, a high concentration of Ang II (1 μM) was required to generate infrequent Ca^{2+} oscillations in isolated JG cells at 1–2 Ca^{2+} spikes per minute. In other cell types (e.g., epithelial cells), Ca^{2+} signaling patterns in intact tissue are more active than those in isolated cells due to the various signaling mechanisms from surrounding tissues, such as exchange of Ca^{2+} or IP3 through gap junction, paracrine signalings mediated by ATP release, or Ca^{2+} influx of stretch-activated channels activated by mechanically coupled cells[61,62]. To study Ca^{2+} dynamics in JG cells while retaining their native structure, we utilized a transgenic mouse approach. *Ren1^c-GCaMP6f* mice exhibit high specificity for JG cells without affecting renin expression, secretion, kidney development, or blood pressure. Using acutely prepared *Ren1^c-GCaMP6f* mouse kidneys, spatiotemporal Ca^{2+} imaging revealed robust Ca^{2+} oscillations coordinated between adjacent JG cells in response to a lower Ang II concentration (3 nM). The imaging analysis revealed a stereotypical burst pattern of consecutive Ca^{2+} spikes, more frequent and active than previously reported in isolated JG cells[19], suggesting that intercellular interactions enhance Ca^{2+} signaling within JG cell clusters.

Intracellular Ca^{2+} concentration is strictly regulated by coordinated crosstalk between multiple ion channels and transporters in the plasma membrane and internal organelles[63,64]. To define the complement of ion channels driving changes in intracellular Ca^{2+} −and thus renin release− in JG cells, we applied various pharmacological screenings to our *ex vivo* Ca^{2+} imaging of JG cells through a continuous perfusion system. Our *ex vivo* Ca^{2+} imaging of JG cells revealed that extracellular Ca^{2+} depletion eliminates Ang II-elicited Ca^{2+} signals. Unexpectedly, the blockade of VDCC and TRP channels reported to be functionally expressed Ca^{2+} channels in JG cells[29,30,35] did not terminate Ca^{2+} spikes. Instead, the blockade of IP3R at the ER and the Ca^{2+}

uptake inlet SERCA markedly suppressed Ang II-elicited Ca^{2+} spikes. In many cell types, intracellular Ca^{2+} signals propagating as waves and oscillations are induced by Ca^{2+} release from the ER through IP3R[48,59]. Both IP3 and Ca^{2+} are required to open IP3R, through which Ca^{2+} released can activate additional, nearby IP3Rs, thus amplifying the Ca^{2+} signal. Ca^{2+} release can propagate to the extent that IP3 is available, forming the pattern of intracellular Ca^{2+} waves and oscillations[60]. Ang II activates AT1R/$G\alpha_{q/11}$ pathways, inducing phospholipase-C and catalyzing the hydrolysis of phosphatidylinositol-4,5-bisphosphate to generate IP3[65,66]. Considering these pathways and our *ex vivo* Ca^{2+} imaging data, these Ca^{2+} waves and oscillations in JG cells could reflect the direct effect of Ca^{2+} release at ER through IP3R. Our data suggest that Ca^{2+} waves and oscillations in JG cells could reflect the direct effect of Ca^{2+} release at ER through IP3R. The partial reduction of Ca^{2+} spikes caused by VDCC and TRPC1/4/5 blockades could be explained by the indirect effect of reduced intracellular Ca^{2+} levels on IP3R opening frequency or failure to replenish intracellular Ca^{2+} lost through plasma membrane Ca^{2+} ATPase (PMCA) and sodium-calcium exchanger (NCX). Further study is needed to clarify the specific roles of distinct VDCC and TRP channels on Ang II-elicited Ca^{2+} dynamics.

The presence of SOC channels in JG cells has been inferred from experiments showing that blocking SERCA increases intracellular Ca^{2+} levels and inhibits renin release in isolated JG cells[5,6,67]. Our *ex vivo* Ca^{2+} imaging confirmed that blocking SERCA increased intracellular fluorescent intensity globally, highlighting the significance of SOCE in JG cells. However, the channels constituting SOCE and their function had not been described in JG cells. In many cell types, STIM/ORAI1 interaction triggers SOCE: STIM proteins at ER sense Ca^{2+} storage depletion and adjust their conformation to activate Ca^{2+} permeable channels comprised of ORAI at plasma membrane[32,33]. Importantly, ORAI/STIM-mediated SOCE contributes to sustaining

Ca^{2+} oscillations via IP3R by transporting extracellular Ca^{2+} into ER[68]. In particular, ORAI2 and ORAI3, which are ORAI1 homologs and form hetero-multimers with ORAI1, have been recently reported to be essential in sustaining Ca^{2+}-oscillations induced by physiological receptor activation[45]. In fact, our pharmacological blockade of ORAI channels targeting ORAI1 and ORAI3 significantly inhibited Ca^{2+} oscillations and alleviated the suppression of renin secretion induced by Ang II in the renin JG cell cluster, while other cell membrane Ca^{2+} channel blockade exhibited no or minor effects on Ca^{2+} signals. Further, studies have also indicated that STIM1/ORAI-mediated Ca^{2+} signals regulate the activity of various transcription factors, including not only certain isoforms of the nuclear factor of activated T-cells (NFAT) but also Creb, c-fos, Egr1, and Mef2 families[69–73]considered to be crucial in the development and identity of JG cells[28,74]. Further experiments using conditional deletion of the ORAI/STIM complex in cells of the renin lineage *in vivo* would provide profound insights into the differentiation and function of the JG cells.

Ca^{2+} spreads across groups of cells by coordinating their oscillations, generating synchronous oscillatory Ca^{2+} signals responsible for integrated multicellular behaviors. The mechanisms underlying intercellular Ca^{2+} propagation depend on the diffusion of an intracellular messenger through gap junctions[5,75,76]. Among the gap junction proteins, connexins (Cxs) function as a conduit for intercellular communication by transferring inorganic ions, including Ca^{2+}, and small signaling molecules, including cAMP, ATP, and IP3[77]. Within the JGA, JG cells are coupled among themselves and their neighboring EC, VSMC, and extraglomerular mesangial cells through gap junctions[20,21]. Functionally, the global and renin cell-specific conditional deletion of Cx40, the most abundant Cxs in JG cells, induces displacement of renin-expressing cells and inhibits negative regulation of renin synthesis and secretion[56,78]. However, despite studies

showing a critical role for cell-to-cell interactions through gap junctions for adequate development and function of JG cells, how gap junction inhibition affects Ca^{2+} dynamics in JG cells has yet to be investigated. Although the mechanism underlying hyperreninemia in Cx40-deleted mice is controversial[79], our *ex vivo* Ca^{2+} imaging data suggest that decreased intracellular Ca^{2+} concentrations may contribute to the phenotype, as pan-gap junction blockade in the JG cell clusters markedly suppresses intra-cellular Ca^{2+} oscillations along with inter-cellular signaling coordination, mitigating the renin secretion inhibition induced by Ang II. This finding suggests that cell-to-cell interactions mediated by gap junctions are essential for maintaining Ca^{2+} activity within JG cell clusters, thereby regulating renin secretion. This essential finding could not be detected in conventional cell cultures using isolated JG cells, further highlighting the functional significance of JGA structure in modulating renin secretion in JG cells.

Clinically, RAS inhibitors markedly increase circulating renin concentrations, while Ca^{2+} channel blockers have only a mild effect on them. Of note, studies of human kidney biopsy samples have shown that long-term treatment with RAS inhibition causes severe concentric hypertrophy of renal arterioles due to the chronic stimulation of JG cells[80], leading to focal renal ischemia, compared with clinical VDCC (amlodipine or cilnidipine) alone[81]. Our *ex vivo* Ca^{2+} imaging of JG cells provides evidence that Ang II is essential to maintain robust ER-derived Ca^{2+} oscillations through extracellular Ca^{2+} uptake via ORAI channels and neighboring cell-to-cell interactions via gap junction within the JG cluster to prevent excessive renin secretion, while VDCC treatments are insufficient to eliminate Ang II-elicited Ca^{2+} oscillation. Understanding the nature of Ang II-elicited Ca^{2+} dynamics in JG cells could lead to safer long-term therapeutic approaches for cardiovascular diseases and hypertension.

We acknowledged a few limitations of this study. First, our *ex vivo* Ca^{2+} imaging in JG cells can not assess the effect of pressure and sympathetic nerve stimulation. It would be interesting to determine *in vivo* whether mechanosensitive channels or sympathetic and sensory nerves can also govern the acute Ang II pressure-induced inhibition of renin secretion in JG cells[82]. *In vivo* intravital imaging for kidney cells using multi-photon microscopy[83,84] may elucidate Ca^{2+} dynamics in JG cells under pressure changes and physiological stress. Second, we could not examine cAMP levels, which directly regulate renin synthesis and secretion in JG cells[6,10] , due to their ubiquitous expression across various kidney cell types, unlike the specific secretion of renin from JG cells. Since Ca^{2+} dynamics differ in isolated JG cells from those in kidney sections, the cAMP dynamics in JG cells should also be distinct in kidney slices. Simultaneous intracellular Ca^{2+} and cAMP imaging in JG cells could provide a more comprehensive understanding of the intracellular signaling pathways that regulate renin synthesis and secretion[85].

In conclusion, our study provides a landscape for understanding the Ca^{2+} dynamics and the relevant ion channels elicited by Ang II in native JG cell clusters and thus may lead to the development of novel therapeutic approaches for cardiovascular and renal diseases in light of their impact on the RAS. Circulating levels of renin are the result of a balance between stimulation and inhibition of renin secretion. Both are crucial to maintaining the appropriate renin levels that maintain normal blood pressure and fluid-electrolyte balance. Overall, this study shows the often overlooked inhibitory step whereby the end product of the RAS cascade, Ang II, exhibits a negative feedback on renin release via a complex regulation of intracellular Ca^{2+} and, in doing so, maintains homeostasis.

Methods

Animals

Ren1^{c}*-Cre* mice, where Cre expression is under the control of the renin promoter[11,23,24], were bred to B6J.Cg-*Gt(ROSA)26Sor*$^{tm95.1(CAG-GCaMP6f)Hze}$*/MwarJ*[25] (Jackson Laboratory, Bar Harbor, ME, Strain #028865) generating mice with JG cell-specific GCaMP6 expression (*Ren1*^{c}*-GCaMP6f* mice; *GCaMP6f*$^{fl/+}$*; Ren1*$^{c\text{-}Cre/+}$). C57BL/6 mice were obtained from the Jackson Laboratory (Strain #000664). Genotyping of the mice was performed by Transnetyx (Cordova, TN). All animals used in this study were maintained in the C57BL/6 background. Mice were group-housed in a temperature and humidity-controlled room under a 12-hour light/dark cycle. All animals were handled according to the National Institutes of Health guidelines for the care and use of experimental animals. The Institutional Animal Care and Use Committee of the University of Virginia approved the study.

Kidney slice preparation

Ren1^{c}*-GCaMP6f* male and female mice between 30 and 100 days of age were anesthetized with tribromoethanol (300 mg/kg, i.p.), and the right kidney was dissected. Kidneys were sectioned (75 μm-thick) in ice-cold PIPES incubation buffer (20 mM PIPES, 119 mM NaCl, 4 mM KCl, 2 mM $CaCl_2$, 1 mM $MgCl_2$, 25 mM D-Glucose, 5 mM $NaHCO_3$, adjusted pH 7.25–7.3 with 10 N NaOH to set Na 154 mM) using Leica VT1200 S fully automated vibrating-blade microtome (Leica, Wetzlar, Germany). Sections were kept at 37 °C for 20 min and then allowed to return to room temperature for the duration of the experiment. PIPES Imaging buffer (20 mM PIPES, 104 mM NaCl, 4 mM KCl, 2 mM $CaCl_2$, 1 mM $MgCl_2$, 25 mM D-Glucose, 0.1% bovine serum

albumin, adjusted pH 7.25–7.3 with 10 N NaOH to set Na 134 mM and 280 mOsm) included with drugs are perfused at a rate of 2.5 mL/min and 37 °C throughout acquisition. The following drugs were used: Angiotensin II (50 pM–300 nM, Thermo Fisher Scientific, Waltham, MA), Nifedipine (10 μM, Sigma-Aldrich, St. Louis, MO), TTA-P2 (10 μM, Merck Millipore, Billerica, MA), SAR7334[41] (10 uM, MedChemExpress, Monmouth Junction, NJ), Pico145[40] (10 uM, MedChemExpress), Ruthenium Red (10 uM, Sigma-Aldrich), Cyclopiazonic acid (20 uM, Cayman Chemicals, Ann Arbor, MI), 2-Aminoethoxydiphenyl borate (100 uM, Thermo Fisher Scientific), Dantrolene (10 uM, MedChemExpress), Gadolinium (5–50 uM, MedChemExpress), GSK-7975A[47] (10 uM, MedChemExpress), and Carbenoxolone (100 uM, Thermo Fisher Scientific).

Calcium image acquisition

Kidney slices were imaged as previously described with minor modification[9,86]. Briefly, kidney slices (75 μm-thick) were imaged in a perfusion buffer on a widefield fluorescence microscope (Zeiss Axio-Examiner, Carl Zeiss Meditec, Dublin, CA) equipped with a 63x water-dipping objective lens, X-Cite XLED light source (Excelitas Technologies Corp., Waltham, MA), and a PM-7D magnetic stage with RC-27L large bath chamber (Warner Instrument Corp., Hamden, CT) configured for a perfusion system. Images were acquired at 10 Hz with an sCMOS camera (Hamamatsu Orca-Flash 4.0) using Slidebook 6 software (Intelligent Imaging Innovations, Denver, CO). Sections were pretreated for ~20 min with Angiotensin II (50 pM–300 nM) before the start of each experiment. For most experiments, a baseline (Ang II-pretreated) 10-minute acquisition period was followed by a 15-minute perfusion of hormone/drug. Slidebook files were converted to high-quality multipage tiffs for analysis using Image J/Fiji[87].

Signal extraction and analysis

Each multi-page Tiff time series was cropped and analyzed using the Mesmerize platform[26] and custom Matlab software. Imaging data were motion-corrected using the CaImAn tool[27], and then, ROIs were detected with CNMF(E)[88,89] under the Mesmerize analysis platform. Ca^{2+} transient spikes in each time series are identified using custom MATLAB software, which combines an automated spike detection algorithm with manual corrections for erroneous or missing spikes. Ca^{2+} activity is presented in raster plots and quantified to determine mean spikes/cell, mean frequency/cell, and bursting activity. To assess manipulation-dependent changes in cellular activity, Ca^{2+} spikes are organized in 1-minute bins and mean spikes/cells are averaged across ROIs within a slice. To quantify the percentage of fluorescent intensity after treatments, the previous report is applied to acquired multi-imaged tiffs with some modifications[90]. Briefly, a hand-drawn ROI was placed around the JG area, the background fluorescence was subtracted, and $\Delta F/F$ of the Baseline period (5–10 minutes) was averaged, and the ratio to averaged $\Delta F/F$ of the Drug period (20–25 minutes) was calculated.

Burst detection

Spikes were grouped into bursts, as we previously reported[9,86]. Briefly, all inter-spike period distribution was fitted with a mixture of Gaussian and exponential distributions. The all inter-spike period value at the intersection of the Gaussian and exponential components of the distribution was taken as a threshold to determine the maximum inter-spike periods within a burst (see also Supplementary Figure 3). Bursts were defined as three or more consecutive Ca^{2+}

spikes within a calculated time threshold from the previous spike. Burst properties (e.g., the number of bursts, spike number, duration) were averaged across individual cells to derive a mean value per slice.

Renin secretion assay

Kidney sections from male C57Bl6/J mice (60–90 days old) were sectioned (75 μm thick) as described under kidney slice preparation. In a 24-well plate, kidney sections were divided into each well in 1.0 mL PIPES imaging buffer. After 15–30 min of incubation (baseline), the solution was sampled (1 mL), and the sections were transferred into the new 24-well plate sample with fresh media containing each concentration of Ang II or drugs. After 30 minutes, a final sample (study) was collected. Renin concentration was determined using ELISA following the manufacturer's instructions (RayBiotech, Norcross, GA). To correct the variation of the number of JG cells in each kidney slice, the renin concentration of study samples was divided by that of each baseline sample, calculated as Fold renin secretion.

Immunohistochemistry/Immunofluorescence staining and histological analysis

GFP expression after Cre recombination was visualized in frozen sections. Mice were anesthetized with tribromoethanol (300 mg/kg). For Immunofluorescence staining for renin, tissues were fixed in 4% paraformaldehyde (PFA) under vacuum for 2 hours at 4°C using a vacuum desiccator. After washing with phosphate-buffered saline (PBS) 2 times, the samples were incubated in 30% D-sucrose/PBS overnight at 4°C and frozen in O.C.T. (Thermo Fisher Scientific). For staining renin, the frozen blocks were sectioned at 8 μm thickness. After washing

with PBS, the sections were post-fixed with 4% PFA for 30 minutes. After the blocking with 3% BSA, 5% donkey serum, and 0.04 % cold fish skin gelatin, sections were incubated with the rabbit monoclonal anti-renin antibody (1:5,000, Abcam, Cambridge, MA, ab212197) at 4 ˚C overnight. After the washing, sections were incubated with Alexa Flour 647 donkey anti-rabbit IgG (1:400, Vector Laboratories, Burlingame, CA, BA-1000) at room temperature for 2 hours. After the washing, sections were incubated with a quencher (Vector TrueView Autofluorescence Quenching Kit #SP-8400, Vector Labs) for 5 min to decrease autofluorescence. Nuclei were stained with Hoechst 33342 (1:5,000, Thermo Fisher Scientific).

For Immunohistochemistry staining for renin and α-smooth muscle actin (α-SMA), tissue sections from paraffin blocks fixed with Bouin's solution were deparaffinized, rehydrated, and treated with 0.3% hydrogen peroxide in methanol. After the blocking with 3% BSA and 2% goat serum or horse serum, sections were incubated with the rabbit polyclonal anti-renin antibody generated in our laboratory (1:500)[12] or the anti-α-SMA antibody (1:10,000, Millipore-Sigma, Burlington, MA, A2547)[91] at 4 ˚C overnight. After the washing, sections were incubated with biotinylated secondary antibody, goat anti-rabbit IgG (1:200, Vector Laboratories, BA-1000) or horse anti-mouse IgG (1:200, Vector Laboratories, BA-2000) for renin or α-SMA, respectively, at room temperature for 30 minutes. Staining was amplified using the Vectastain ABC kit (Vector Laboratories) and developed with 3,3'-diaminobenzidine (Millipore-Sigma)[92]. The sections were counterstained with hematoxylin (Millipore-Sigma), dehydrated, and mounted with Cytoseal XYL (Thermo Fisher Scientific). Images were captured using a Zeiss Imager M2 microscope equipped with an ApoTome2 with an AxioCam 506 mono and an AxioCam 305 color camera (Carl Zeiss Co., Oberkochen, Germany).

The JGA index was determined as the percentage of renin-positive JGAs per total glomeruli[74,93–95]. We counted the number of renin-expressing cells in each JGA and along the arterioles with visible glomeruli attached to determine the number of renin-expressing cells per section.

ELISA for renin in plasma

Plasma specimens were obtained from blood after centrifugation at 1,000 g at 4 ˚C for 20 minutes. Renin concentration was determined using ELISA (RayBiotech)[94].

RNA extraction and quantitative RT-PCR

Renal cortices were removed and placed in RNAlater Stabilization Solution (Thermo Fisher Scientific) overnight at 4°C and then stored at −20°C. RNA was extracted from renal cortices using TRIzol reagent (Thermo Fisher Scientific). Reverse transcription (RT) was performed using oligo(dT) primer and M-MLV Reverse Transcriptase (Promega, Madison, WI) according to the manufacturer's instructions. Quantitative PCR was performed with SYBR Green I (Thermo Fisher Scientific) in a CFX Connect system (Bio-Rad Laboratories, Hercules, CA). PCR was performed using the following primers: *Ren1*, forward: 5'-ACAGTATCCCAACAGGAGAGACAAG-3', reverse: 5'-GCACCCAGGACCCAGACA-3'; *Rps14*, forward: 5'-CAGGACCAAGACCCCTGGA-3', reverse: 5'-ATCTTCATCCCAGAGCGAGC-3'. The mRNA expression was normalized to *Rps14* expression, and the changes in expression were determined by the ΔΔCt method and were reported as relative expression compared to control mice[96].

Carotid arterial pressure measurement

Anesthetized mice were kept at 37.5°C with 2.0% isoflurane inhalation. Heparinized saline-filled polyethylene catheters (PE10, Becton Dickinson; 0.28 mm internal diameter) were inserted into the right carotid artery using an RX104A transducer coupled to a data acquisition system and AcqKnowledge software (Biopac Systems, Inc., Goleta, CA). Blood pressure was continuously recorded for over 10 minutes to measure the mean arterial pressure[74,80].

Bubble plot for single-cell RNA sequence

Our previous single-cell RNA sequencing data from embryonic and adult *FoxD1*$^{cre/+}$*; R26R-mTmG* mice kidneys (GSE218570[28]) was used for dot plot visualization of L-type and T-type VDCC α_1-subunits, canonical TRP (TRPC) and vanilloid TRP (TRPV) subfamilies, ORAI/STIM complex, endoplasmic reticulum channels, and gap junction protein genes set in renin-lineage cells. The dot plot was produced using custom versions of the functions from https://renin-analysis.readthedocs.io/en/latest/18.R_generate_bubble_plots/. The input to the calcBubble() function was the raw gene expression matrix. The input matrix was then log normalized and z-score transformed with the percentage of cells of each population expressing each gene calculated along with the z-scores for each gene across all cell populations in the gene expression matrix. The output from this function was then plotted using ggplot2[97].

Statistical Analysis

Statistical analyses were performed using GraphPad Prism software (ver10.2.3) and R (ver4.4.1). Based on the test requirements, Student's two-tailed t-test, Mann-Whitney U test, one-way ANOVA with Šídák's multi-comparison test, one-way ANOVA with Tukey's multi-comparison test, two-way ANOVA with Šídák's multi-comparison test, and linear mixed model. Statistical tests and results are shown in Figure legends. $P<0.05$ was considered significant. Data are shown as mean ± SEM. Schematics created with BioRender.com.

The hypotheses were tested by using a linear mixed model analysis that accounts for within-subject correlation of pseudoreplicates. The multi-level analysis's number of pseudoreplicates (ROIs/slice) and genuine replicates (mice) is reported in each figure legend where applicable. For Ca^{2+} imaging studies in which each mouse contributed exactly one slice per experimental condition, the mouse is considered a genuine replicate, while the slice and every ROI within the slice are considered pseudoreplicates. Therefore, the correlated error was modeled using a hierarchical structure, with mouse > slice > ROI.

Data Availability

All supporting data are available within the article and its supplementary files. Additional information will be available upon request to the corresponding authors.

Acknowledgments

We thank Thomas Wagamon for their excellent technical assistance.

Author contributions

H.Y., N.A.G., R.A.G., and M.L.S.S.-L. conceived and designed research; H.Y. and N.A.G. performed Kidney slice preparation, Calcium image acquisition, Signal extraction and analysis, and Burst detection; H.Y. performed Renin secretion assay, Plasma collection, Immunohistochemistry staining, RNA extraction, quantitative RT-PCR, and Carotid arterial pressure measurement; F.X. performed Renin ELISA for renin secretion assay and plasma; H.Y. and M.Y. performed immunofluorescence staining; H.Y. analyzed data; H.Y. and J.P.S. analyzed single-cell RNA sequence data and generated Bubble plots; H.Y. S.M., N.A.G, R.A.G., and M.L.S.S.-L. interpreted results of experiments; H.Y. prepared figures; H.Y. drafted manuscript; H.Y., M.Y., J.P.S., L.F.A., D.M, S.M., N.A.G, R.A.G., and M.L.S.S.-L. edited and revised manuscript; H.Y., M.Y., J.P.S., L.F.A., D.M, S.M., N.A.G, R.A.G., and M.L.S.S.-L. approved final version of the manuscript.

Competing interests

The authors declare no competing interest.

Grants

This work was supported by National Institutes of Health Grants P50DK096373, R01DK116718, and R01HL148044 to R.A.G. and M.L.S.S.-L.

References

1. Gomez RA, Sequeira-Lopez MLS. Renin cells in homeostasis, regeneration and immune defence mechanisms. *Nat Rev Nephrol*. 2018;14(4):231-245. doi:10.1038/nrneph.2017.186

2. Yamaguchi H, Gomez RA, Sequeira-Lopez MLS. Renin Cells, From Vascular Development to Blood Pressure Sensing. *Hypertension*. Published online 2023. doi:10.1161/hypertensionaha.123.20577

3. Sequeira-Lopez MLS, Gomez RA. Renin Cells, the Kidney, and Hypertension. *Circ Res*. 2021;128(7):887-907. doi:10.1161/circresaha.121.318064

4. Yamaguchi M, Almeida LF de, Yamaguchi H, Liang X, Smith JP, Medrano S, Lopez MLSS, Gomez RA. Transformation of the Kidney into a Pathological Neuro-Immune-Endocrine Organ. *Circ Res*. Published online 2024. doi:10.1161/circresaha.124.325305

5. Yao J, Suwa M, Li B, Kawamura K, Morioka T, Oite T. ATP-Dependent Mechanism for Coordination of Intercellular Ca2+ Signaling and Renin Secretion in Rat Juxtaglomerular Cells. *Circ Res*. 2003;93(4):338-345. doi:10.1161/01.res.0000086802.21850.5d

6. Grünberger C, Obermayer B, Klar J, Kurtz A, Schweda F. The Calcium Paradoxon of Renin Release. *Circ Res*. 2006;99(11):1197-1206. doi:10.1161/01.res.0000251057.35537.d3

7. Beierwaltes WH. The role of calcium in the regulation of renin secretion. *Am J Physiol-renal*. 2010;298(1):F1-F11. doi:10.1152/ajprenal.00143.2009

8. Rorsman P, Braun M, Zhang Q. Regulation of calcium in pancreatic α- and β-cells in health and disease. *Cell Calcium*. 2012;51(3-4):300-308. doi:10.1016/j.ceca.2011.11.006

9. Guagliardo NA, Klein PM, Gancayco CA, Lu A, Leng S, Makarem RR, Cho C, Rusin CG, Breault DT, Barrett PQ, Beenhakker MP. Angiotensin II induces coordinated calcium bursts in aldosterone-producing adrenal rosettes. *Nat Commun*. 2020;11(1):1679. doi:10.1038/s41467-020-15408-4

10. Kurtz A. Renin Release: Sites, Mechanisms, and Control. *Annu Rev Physiol*. 2011;73(1):377-399. doi:10.1146/annurev-physiol-012110-142238

11. Pentz ES, Lopez MLSS, Cordaillat M, Gomez RA. Identity of the renin cell is mediated by cAMP and chromatin remodeling: an in vitro model for studying cell recruitment and plasticity. *Am J Physiol-heart C*. 2008;294(2):H699-H707. doi:10.1152/ajpheart.01152.2007

12. Gomez RA, Pentz ES, Jin X, Cordaillat M, Lopez MLSS. CBP and p300 are essential for renin cell identity and morphological integrity of the kidney. *Am J Physiol-heart C*. 2009;296(5):H1255-H1262. doi:10.1152/ajpheart.01266.2008

13. Neubauer B, Machura K, Chen M, Weinstein LS, Oppermann M, Sequeira-Lopez ML, Gomez RA, Schnermann J, Castrop H, Kurtz A, Wagner C. Development of vascular renin expression in the kidney critically depends on the cyclic AMP pathway. *Am J Physiol-renal*. 2009;296(5):F1006-F1012. doi:10.1152/ajprenal.90448.2008

14. Smith JP, Paxton R, Medrano S, Sheffield NC, Sequeira-Lopez MLS, Gomez RA. Inhibition of Renin Expression Is Regulated by an Epigenetic Switch From an Active to a Poised State. *Hypertension*. 2024;81(9):1869-1882. doi:10.1161/hypertensionaha.124.22886

15. Forrester SJ, Booz GW, Sigmund CD, Coffman TM, Kawai T, Rizzo V, Scalia R, Eguchi S. Angiotensin II Signal Transduction: An Update on Mechanisms of Physiology and Pathophysiology. *Physiol Rev*. 2018;98(3):1627-1738. doi:10.1152/physrev.00038.2017

16. Neubauer B, Schrankl J, Steppan D, Neubauer K, Sequeira-Lopez ML, Pan L, Gomez RA, Coffman TM, Gross KW, Kurtz A, Wagner C. Angiotensin II Short-Loop Feedback. *Hypertension*. 2018;71(6):1075-1082. doi:10.1161/hypertensionaha.117.10357

17. Naftilan AJ, Oparil S. Inhibition of renin release from rat kidney slices by the angiotensins. *Am J Physiol-Ren Physiol*. 1978;235(1):F62-F68. doi:10.1152/ajprenal.1978.235.1.f62

18. Kurtz A, Pfeilschifter J, Hutter A, Buhrle C, Nobiling R, Taugner R, Hackenthal E, Bauer C. Role of protein kinase C in inhibition of renin release caused by vasoconstrictors. *Am J Physiol-Cell Physiol*. 1986;250(4):C563-C571. doi:10.1152/ajpcell.1986.250.4.c563

19. Kurtz A, Penner R. Angiotensin II induces oscillations of intracellular calcium and blocks anomalous inward rectifying potassium current in mouse renal juxtaglomerular cells. *Proc Natl Acad Sci*. 1989;86(9):3423-3427. doi:10.1073/pnas.86.9.3423

20. Taugner R, Schiller A, Kaissling B, Kriz W. Gap junctional coupling between the JGA and the glomerular tuft. *Cell Tissue Res*. 1978;186(2):279-285. doi:10.1007/bf00225537

21. Castrop H, Höcherl K, Kurtz A, Schweda F, Todorov V, Wagner C. Physiology of Kidney Renin. *Physiol Rev*. 2010;90(2):607-673. doi:10.1152/physrev.00011.2009

22. Karginova EA, Pentz ES, Kazakova IG, Norwood VF, Carey RM, Gomez RA. Zis: a developmentally regulated gene expressed in juxtaglomerular cells. *Am J Physiol-renal*. 1997;273(5):F731-F738. doi:10.1152/ajprenal.1997.273.5.f731

23. Brunskill EW, Sequeira-Lopez MLS, Pentz ES, Lin E, Yu J, Aronow BJ, Potter SS, Gomez RA. Genes that Confer the Identity of the Renin Cell. *J Am Soc Nephrol*. 2011;22(12):2213-2225. doi:10.1681/asn.2011040401

24. Oka M, Medrano S, Sequeira-López MLS, Gómez RA. Chronic Stimulation of Renin Cells Leads to Vascular Pathology. *Hypertension*. 2018;70(1):119-128. doi:10.1161/hypertensionaha.117.09283

25. Madisen L, Garner AR, Shimaoka D, Chuong AS, Klapoetke NC, Li L, van der Bourg A, Niino Y, Egolf L, Monetti C, Gu H, Mills M, Cheng A, Tasic B, Nguyen TN, Sunkin SM, Benucci A, Nagy A, Miyawaki A, Helmchen F, Empson RM, Knöpfel T, Boyden ES, Reid RC, Carandini M, Zeng H. Transgenic Mice for Intersectional Targeting of Neural Sensors and Effectors with High Specificity and Performance. *Neuron*. 2015;85(5):942-958. doi:10.1016/j.neuron.2015.02.022

26. Kolar K, Dondorp D, Zwiggelaar JC, Høyer J, Chatzigeorgiou M. Mesmerize is a dynamically adaptable user-friendly analysis platform for 2D and 3D calcium imaging data. *Nat Commun*. 2021;12(1):6569. doi:10.1038/s41467-021-26550-y

27. Giovannucci A, Friedrich J, Gunn P, Kalfon J, Brown BL, Koay SA, Taxidis J, Najafi F, Gauthier JL, Zhou P, Khakh BS, Tank DW, Chklovskii DB, Pnevmatikakis EA. CaImAn an open source tool for scalable calcium imaging data analysis. *eLife*. 2019;8:e38173. doi:10.7554/elife.38173

28. Martini AG, Smith JP, Medrano S, Finer G, Sheffield NC, Sequeira-Lopez MLS, Gomez RA. Renin Cell Development: Insights From Chromatin Accessibility and Single-Cell Transcriptomics. *Circ Res*. Published online 2023. doi:10.1161/circresaha.123.322827

29. Ortiz-Capisano MC, Atchison DK, Harding P, Lasley RD, Beierwaltes WH. Adenosine inhibits renin release from juxtaglomerular cells via an A1 receptor-TRPC-mediated pathway. *Am J Physiol-Ren Physiol*. 2013;305(8):F1209-F1219. doi:10.1152/ajprenal.00710.2012

30. Seghers F, Yerna X, Zanou N, Devuyst O, Vennekens R, Nilius B, Gailly P. TRPV4 participates in pressure-induced inhibition of renin secretion by juxtaglomerular cells. *J Physiology*. 2016;594(24):7327-7340. doi:10.1113/jp273595

31. Ortiz-Capisano MC. Endothelin inhibits renin release from juxtaglomerular cells via endothelin receptors A and B via a transient receptor potential canonical-mediated pathway. *Physiol Rep*. 2014;2(12):e12240. doi:10.14814/phy2.12240

32. Prakriya M, Feske S, Gwack Y, Srikanth S, Rao A, Hogan PG. Orai1 is an essential pore subunit of the CRAC channel. *Nature*. 2006;443(7108):230-233. doi:10.1038/nature05122

33. Cahalan MD, Zhang SL, Yeromin AV, Ohlsen K, Roos J, Stauderman KA. Molecular basis of the CRAC channel. *Cell Calcium*. 2007;42(2):133-144. doi:10.1016/j.ceca.2007.03.002

34. Catterall WA. Structure and Regulation of Voltage-Gated Ca2+ Channels. *Annu Rev Cell Dev Biol*. 2000;16(1):521-555. doi:10.1146/annurev.cellbio.16.1.521

35. Friis UG, Jørgensen F, Andreasen D, Jensen BL, Skøtt O. Molecular and Functional Identification of Cyclic AMP-Sensitive BKCa Potassium Channels (ZERO Variant) and L-Type Voltage-Dependent Calcium Channels in Single Rat Juxtaglomerular Cells. *Circ Res*. 2003;93(3):213-220. doi:10.1161/01.res.0000085041.70276.3d

36. Perez-Reyes E. Molecular Physiology of Low-Voltage-Activated T-type Calcium Channels. *Physiol Rev*. 2003;83(1):117-161. doi:10.1152/physrev.00018.2002

37. Stengel W, Jainz M, Andreas K. Different potencies of dihydropyridine derivatives in blocking T-type but not L-type Ca2+ channels in neuroblastoma-glioma hybrid cells. *Eur J Pharmacol*. 1998;342(2-3):339-345. doi:10.1016/s0014-2999(97)01495-7

38. Shipe WD, Barrow JC, Yang ZQ, Lindsley CW, Yang FV, Schlegel KAS, Shu Y, Rittle KE, Bock MG, Hartman GD, Tang C, Ballard JE, Kuo Y, Adarayan ED, Prueksaritanont T, Zrada MM, Uebele VN, Nuss CE, Connolly TM, Doran SM, Fox SV, Kraus RL, Marino MJ, Graufelds VK, Vargas HM, Bunting PB, Hasbun-Manning M, Evans RM, Koblan KS, Renger JJ. Design, Synthesis, and Evaluation of a Novel 4-Aminomethyl-4-fluoropiperidine as a T-Type Ca2+ Channel Antagonist. *J Med Chem*. 2008;51(13):3692-3695. doi:10.1021/jm800419w

39. Hofmann T, Schaefer M, Schultz G, Gudermann T. Subunit composition of mammalian transient receptor potential channels in living cells. *Proc Natl Acad Sci*. 2002;99(11):7461-7466. doi:10.1073/pnas.102596199

40. Rubaiy HN, Ludlow MJ, Henrot M, Gaunt HJ, Miteva K, Cheung SY, Tanahashi Y, Hamzah N, Musialowski KE, Blythe NM, Appleby HL, Bailey MA, McKeown L, Taylor R, Foster R, Waldmann H, Nussbaumer P, Christmann M, Bon RS, Muraki K, Beech DJ. Picomolar, selective, and subtype-specific small-molecule inhibition of TRPC1/4/5 channels. *J Biol Chem*. 2017;292(20):8158-8173. doi:10.1074/jbc.m116.773556

41. Maier T, Follmann M, Hessler G, Kleemann H, Hachtel S, Fuchs B, Weissmann N, Linz W, Schmidt T, Löhn M, Schroeter K, Wang L, Rütten H, Strübing C. Discovery of the novel TRPC6 inhibitor SAR7334. *Br J Pharmacol*. 2015;172(14):3650-3660. doi:10.1111/bph.13151

42. Pumroy RA, Jesús-Pérez JJD, Protopopova AD, Rocereta JA, Fluck EC, Fricke T, Lee BH, Rohacs T, Leffler A, Moiseenkova-Bell V. Molecular details of ruthenium red pore block in TRPV channels. *EMBO Rep*. 2024;25(2):506-523. doi:10.1038/s44319-023-00050-0

43. Trebak M, Bird GStJ, McKay RR, Putney JW. Comparison of Human TRPC3 Channels in Receptor-activated and Store-operated Modes. Differential sensitivity to channel blockers suggests fundamental differences in channel composition. *J Biol Chem*. 2002;277(24):21617-21623. doi:10.1074/jbc.m202549200

44. Yeromin AV, Zhang SL, Jiang W, Yu Y, Safrina O, Cahalan MD. Molecular identification of the CRAC channel by altered ion selectivity in a mutant of Orai. *Nature*. 2006;443(7108):226-229. doi:10.1038/nature05108

45. Yoast RE, Emrich SM, Zhang X, Xin P, Johnson MT, Fike AJ, Walter V, Hempel N, Yule DI, Sneyd J, Gill DL, Trebak M. The native ORAI channel trio underlies the diversity of Ca2+ signaling events. *Nat Commun*. 2020;11(1):2444. doi:10.1038/s41467-020-16232-6

46. Bouron A, Kiselyov K, Oberwinkler J. Permeation, regulation and control of expression of TRP channels by trace metal ions. *Pflügers Arch - Eur J Physiol*. 2015;467(6):1143-1164. doi:10.1007/s00424-014-1590-3

47. Derler I, Schindl R, Fritsch R, Heftberger P, Riedl MC, Begg M, House D, Romanin C. The action of selective CRAC channel blockers is affected by the Orai pore geometry. *Cell Calcium*. 2013;53(2):139-151. doi:10.1016/j.ceca.2012.11.005

48. Narayanan D, Adebiyi A, Jaggar JH. Inositol trisphosphate receptors in smooth muscle cells. *Am J Physiol-Hear Circ Physiol*. 2012;302(11):H2190-H2210. doi:10.1152/ajpheart.01146.2011

49. Moncoq K, Trieber CA, Young HS. The Molecular Basis for Cyclopiazonic Acid Inhibition of the Sarcoplasmic Reticulum Calcium Pump*. *J Biol Chem*. 2007;282(13):9748-9757. doi:10.1074/jbc.m611653200

50. Venkatachalam K, Rossum DB van, Patterson RL, Ma HT, Gill DL. The cellular and molecular basis of store-operated calcium entry. *Nat Cell Biol*. 2002;4(11):E263-E272. doi:10.1038/ncb1102-e263

51. Maruyama T, Kanaji T, Nakade S, Kanno T, Mikoshiba K. 2APB, 2-Aminoethoxydiphenyl Borate, a Membrane-Penetrable Modulator of Ins(1,4,5)P3-Induced Ca2+ Release. *J Biochem*. 1997;122(3):498-505. doi:10.1093/oxfordjournals.jbchem.a021780

52. Zhao F, Li P, Chen SRW, Louis CF, Fruen BR. Dantrolene Inhibition of Ryanodine Receptor Ca2+ Release Channels. Molecular mechanism and isoform selectivity. *J Biol Chem*. 2001;276(17):13810-13816. doi:10.1074/jbc.m006104200

53. Xu L, Tripathy A, Pasek DA, Meissner G. Ruthenium Red Modifies the Cardiac and Skeletal Muscle Ca2+ Release Channels (Ryanodine Receptors) by Multiple Mechanisms*. *J Biol Chem*. 1999;274(46):32680-32691. doi:10.1074/jbc.274.46.32680

54. Prakriya M, Lewis RS. Potentiation and inhibition of Ca2+ release-activated Ca2+ channels by 2-aminoethyldiphenyl borate (2-APB) occurs independently of IP3 receptors. *J Physiol*. 2001;536(1):3-19. doi:10.1111/j.1469-7793.2001.t01-1-00003.x

55. Wagner C, Wit C de, Kurtz L, Grünberger C, Kurtz A, Schweda F. Connexin40 Is Essential for the Pressure Control of Renin Synthesis and Secretion. *Circ Res*. 2007;100(4):556-563. doi:10.1161/01.res.0000258856.19922.45

56. Wagner C, Jobs A, Schweda F, Kurtz L, Kurt B, Lopez MLS, Gomez RA, Veen TAB van, Wit C de, Kurtz A. Selective deletion of Connexin 40 in renin-producing cells impairs renal baroreceptor function and is associated with arterial hypertension. *Kidney Int*. 2010;78(8):762-768. doi:10.1038/ki.2010.257

57. DeLalio LJ, Masati E, Mendu S, Ruddiman CA, Yang Y, Johnstone SR, Milstein JA, Keller TCS, Weaver RB, Guagliardo NA, Best AK, Ravichandran KS, Bayliss DA, Sequeira-Lopez

MLS, Sonkusare SN, Shu XH, Desai B, Barrett PQ, Le TH, Gomez RA, Isakson BE. Pannexin 1 channels in renin-expressing cells influence renin secretion and blood pressure homeostasis. *Kidney Int*. 2020;98(3):630-644. doi:10.1016/j.kint.2020.04.041

58. Juszczak GR, Swiergiel AH. Properties of gap junction blockers and their behavioural, cognitive and electrophysiological effects: Animal and human studies. *Prog Neuro-Psychopharmacol Biol Psychiatry*. 2009;33(2):181-198. doi:10.1016/j.pnpbp.2008.12.014

59. Berridge MJ, Bootman MD, Roderick HL. Calcium signalling: dynamics, homeostasis and remodelling. *Nat Rev Mol Cell Biol*. 2003;4(7):517-529. doi:10.1038/nrm1155

60. Iino M. Spatiotemporal dynamics of Ca2+ signaling and its physiological roles. *Proc Jpn Acad, Ser B*. 2010;86(3):244. doi:10.2183/pjab.86.244

61. Leybaert L, Sanderson MJ. Intercellular Ca2+ Waves: Mechanisms and Function. *Physiol Rev*. 2012;92(3):1359-1392. doi:10.1152/physrev.00029.2011

62. Balaji R, Bielmeier C, Harz H, Bates J, Stadler C, Hildebrand A, Classen AK. Calcium spikes, waves and oscillations in a large, patterned epithelial tissue. *Sci Rep*. 2017;7(1):42786. doi:10.1038/srep42786

63. Berridge MJ, Lipp P, Bootman MD. The versatility and universality of calcium signalling. *Nat Rev Mol Cell Biol*. 2000;1(1):11-21. doi:10.1038/35036035

64. Clapham DE. Calcium Signaling. *Cell*. 2007;131(6):1047-1058. doi:10.1016/j.cell.2007.11.028

65. Guo DF, Sun YL, Hamet P, Inagami T. The angiotensin II type 1 receptor and receptor-associated proteins. *Cell Res*. 2001;11(3):165-180. doi:10.1038/sj.cr.7290083

66. Hunyady L, Catt KJ. Pleiotropic AT1 Receptor Signaling Pathways Mediating Physiological and Pathogenic Actions of Angiotensin II. *Mol Endocrinol*. 2006;20(5):953-970. doi:10.1210/me.2004-0536

67. Schweda F, Riegger GAJ, Kurtz A, Krämer BK. Store-operated calcium influx inhibits renin secretion. *Am J Physiol-Ren Physiol*. 2000;279(1):F170-F176. doi:10.1152/ajprenal.2000.279.1.f170

68. Putney JW. Calcium Signaling: Deciphering the Calcium–NFAT Pathway. *Curr Biol*. 2012;22(3):R87-R89. doi:10.1016/j.cub.2011.12.030

69. Pulver-Kaste RA, Barlow CA, Bond J, Watson A, Penar PL, Tranmer B, Lounsbury KM. Ca2+ source-dependent transcription of CRE-containing genes in vascular smooth muscle. *Am J Physiol-Hear Circ Physiol*. 2006;291(1):H97-H105. doi:10.1152/ajpheart.00753.2005

70. Ren J, Albinsson S, Hellstrand P. Distinct Effects of Voltage- and Store-dependent Calcium Influx on Stretch-induced Differentiation and Growth in Vascular Smooth Muscle*. *J Biol Chem*. 2010;285(41):31829-31839. doi:10.1074/jbc.m109.097576

71. Darbellay B, Arnaudeau S, König S, Jousset H, Bader C, Demaurex N, Bernheim L. STIM1- and Orai1-dependent Store-operated Calcium Entry Regulates Human Myoblast Differentiation*. *J Biol Chem*. 2009;284(8):5370-5380. doi:10.1074/jbc.m806726200

72. Simo-Cheyou ER, Tan JJ, Grygorczyk R, Srivastava AK. STIM-1 and ORAI-1 channel mediate angiotensin-II-induced expression of Egr-1 in vascular smooth muscle cells. *J Cell Physiol*. 2017;232(12):3496-3509. doi:10.1002/jcp.25810

73. Nieto-Felipe J, Macias-Diaz A, Sanchez-Collado J, Berna-Erro A, Jardin I, Salido GM, Lopez JJ, Rosado JA. Role of Orai-family channels in the activation and regulation of transcriptional activity. *J Cell Physiol*. 2023;238(4):714-726. doi:10.1002/jcp.30971

74. Martinez MF, Medrano S, Brown EA, Tufan T, Shang S, Bertoncello N, Guessoum O, Adli M, Belyea BC, Lopez MLSS, Gomez RA. Super-enhancers maintain renin-expressing cell identity and memory to preserve multisystem homeostasis. *J Clin Invest*. 2018;128(11):4787-4803. doi:10.1172/jci121361

75. Jørgensen NR, Geist ST, Civitelli R, Steinberg TH. ATP- and Gap Junction–dependent Intercellular Calcium Signaling in Osteoblastic Cells. *J Cell Biol*. 1997;139(2):497-506. doi:10.1083/jcb.139.2.497

76. Røttingen, Iversen. Ruled by waves? Intracellular and intercellular calcium signalling. *Acta Physiol Scand*. 2000;169(3):203-219. doi:10.1046/j.1365-201x.2000.00732.x

77. Dbouk HA, Mroue RM, El-Sabban ME, Talhouk RS. Connexins: a myriad of functions extending beyond assembly of gap junction channels. *Cell Commun Signal*. 2009;7(1):4. doi:10.1186/1478-811x-7-4

78. Kurtz L, Schweda F, Wit C de, Kriz W, Witzgall R, Warth R, Sauter A, Kurtz A, Wagner C. Lack of Connexin 40 Causes Displacement of Renin-Producing Cells from Afferent Arterioles to the Extraglomerular Mesangium. *J Am Soc Nephrol*. 2007;18(4):1103-1111. doi:10.1681/asn.2006090953

79. Gomez RA, Lopez MLSS. Who and where is the renal baroreceptor?: the connexin hypothesis. *Kidney Int*. 2009;75(5):460-462. doi:10.1038/ki.2008.536

80. Watanabe H, Martini AG, Brown EA, Liang X, Medrano S, Goto S, Narita I, Arend LJ, Sequeira-Lopez MLS, Gomez RA. Inhibition of the renin-angiotensin system causes concentric hypertrophy of renal arterioles in mice and humans. *Jci Insight*. 2021;6(24):e154337. doi:10.1172/jci.insight.154337

81. Nagai Y, Yamabe F, Sasaki Y, Ishii T, Nakanishi K, Nakajima K, Shibuya K, Mikami T, Akasaka Y, Urita Y, Yamanaka N. A Study of Morphological Changes in Renal Afferent Arterioles Induced by Angiotensin II Type 1 Receptor Blockers in Hypertensive Patients. *Kidney Blood Press Res*. 2020;45(2):194-208. doi:10.1159/000505025

82. Nagalakshmi VK, Smith JP, Matsuoka D, Gomez RA, Sequeira-Lopez MLS. Piezo channels in JG cells do not regulate renin expression or renin release to the circulation. *Clin Sci*. 2024;138(23):1527-1536. doi:10.1042/cs20242089

83. Hackl MJ, Burford JL, Villanueva K, Lam L, Suszták K, Schermer B, Benzing T, Peti-Peterdi J. Tracking the fate of glomerular epithelial cells in vivo using serial multiphoton imaging in new mouse models with fluorescent lineage tags. *Nat Med*. 2013;19(12):1661-1666. doi:10.1038/nm.3405

84. Binz-Lotter J, Jüngst C, Rinschen MM, Koehler S, Zentis P, Schauss A, Schermer B, Benzing T, Hackl MJ. Injured Podocytes Are Sensitized to Angiotensin II–Induced Calcium Signaling. *J Am Soc Nephrol*. 2020;31(3):532-542. doi:10.1681/asn.2019020109

85. Yokoyama T, Manita S, Uwamori H, Tajiri M, Imayoshi I, Yagishita S, Murayama M, Kitamura K, Sakamoto M. A multicolor suite for deciphering population coding of calcium and cAMP in vivo. *Nat Methods*. 2024;21(5):897-907. doi:10.1038/s41592-024-02222-9

86. Gancayco CA, Gerding MR, Breault DT, Beenhakker MP, Barrett PQ, Guagliardo NA. Intrinsic Adrenal TWIK-Related Acid-Sensitive TASK Channel Dysfunction Produces Spontaneous Calcium Oscillations Sufficient to Drive AngII (Angiotensin II)-Unresponsive Hyperaldosteronism. *Hypertension*. 2022;79(11):2552-2564. doi:10.1161/hypertensionaha.122.19557

87. Schindelin J, Arganda-Carreras I, Frise E, Kaynig V, Longair M, Pietzsch T, Preibisch S, Rueden C, Saalfeld S, Schmid B, Tinevez JY, White DJ, Hartenstein V, Eliceiri K, Tomancak P, Cardona A. Fiji: an open-source platform for biological-image analysis. *Nature Methods*. 2012;9(7):676-682. doi:10.1038/nmeth.2019

88. Zhou P, Resendez SL, Rodriguez-Romaguera J, Jimenez JC, Neufeld SQ, Giovannucci A, Friedrich J, Pnevmatikakis EA, Stuber GD, Hen R, Kheirbek MA, Sabatini BL, Kass RE, Paninski L. Efficient and accurate extraction of in vivo calcium signals from microendoscopic video data. *eLife*. 2018;7:e28728. doi:10.7554/elife.28728

89. Tran LM, Mocle AJ, Ramsaran AI, Jacob AD, Frankland PW, Josselyn SA. Automated Curation of CNMF-E-Extracted ROI Spatial Footprints and Calcium Traces Using Open-Source AutoML Tools. *Front Neural Circuits*. 2020;14:42. doi:10.3389/fncir.2020.00042

90. Muto A, Ohkura M, Abe G, Nakai J, Kawakami K. Real-Time Visualization of Neuronal Activity during Perception. *Curr Biol*. 2013;23(4):307-311. doi:10.1016/j.cub.2012.12.040

91. Sequeira-Lopez MLS, Lin EE, Li M, Hu Y, Sigmund CD, Gomez RA. The earliest metanephric arteriolar progenitors and their role in kidney vascular development. *Am J Physiology-regulatory Integr Comp Physiology*. 2015;308(2):R138-R149. doi:10.1152/ajpregu.00428.2014

92. Lin EE, Sequeira-Lopez MLS, Gomez RA. RBP-J in FOXD1+ renal stromal progenitors is crucial for the proper development and assembly of the kidney vasculature and glomerular mesangial cells. *Am J Physiol-renal*. 2014;306(2):F249-F258. doi:10.1152/ajprenal.00313.2013

93. Guessoum O, Zainab M, Sequeira-Lopez MLS, Gomez RA. Proliferation does not contribute to murine models of renin cell recruitment. *Acta Physiol*. 2020;230(3):e13532. doi:10.1111/apha.13532

94. Martinez MF, Martini AG, Sequeira-Lopez MLS, Gomez RA. Ctcf is required for renin expression and maintenance of the structural integrity of the kidney. *Clin Sci*. 2020;134(13):1763-1774. doi:10.1042/cs20200184

95. Neyra JS, Medrano S, Martini ADG, Sequeira-Lopez MLS, Gomez RA. The Role of Gata3 in Renin Cell Identity. *Am J Physiol-Ren Physiol*. Published online 2023. doi:10.1152/ajprenal.00098.2023

96. Tufro-McReddie A, Chevalier RL, Everett AD, Gomez RA. Decreased perfusion pressure modulates renin and ANG II type 1 receptor gene expression in the rat kidney. *Am J Physiology-regulatory Integr Comp Physiology*. 1993;264(4):R696-R702. doi:10.1152/ajpregu.1993.264.4.r696

97. Wickham H. *Ggplot2: Elegant Graphics for Data Analysis. Springer-Verlag New York.*; 2016. Accessed September 30, 2024. https://link.springer.com/book/10.1007/978-3-319-24277-4

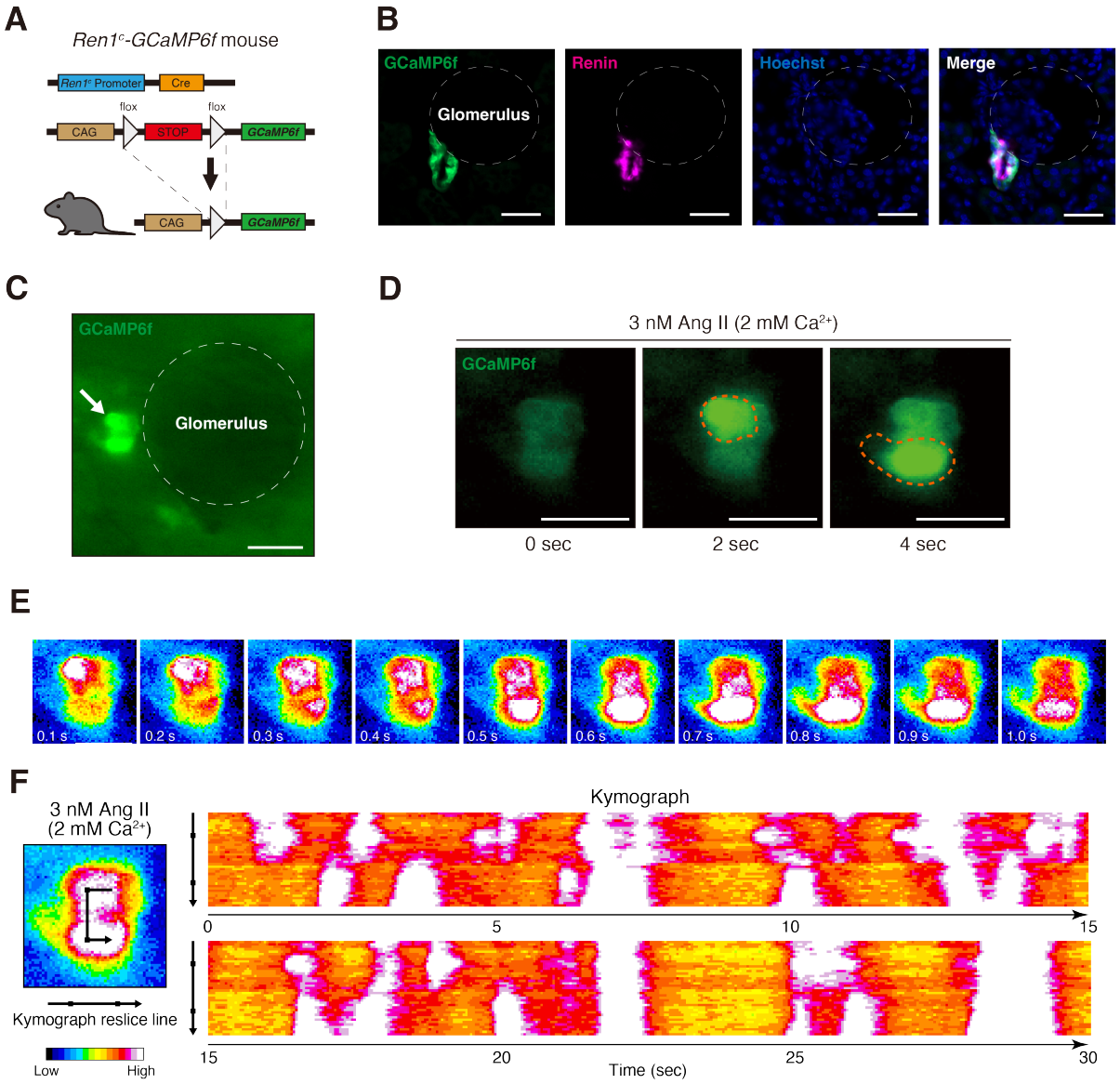

Figure 1. Ang II elicits robust and periodic Ca^{2+}-oscillations within JG cell clusters expressing GCaMP6f.

A, Schematic representation of the generation of GCaMP6f mouse line expressing GCaMP6f exclusively in the renin lineage (*Ren1^c-GCaMP6f* mice). *GCaMP6f$^{fl/fl}$* transgenic mouse contain floxed-STOP cassette inserted upstream of the GCaMP6 fast variant Ca^{2+} indicator (GCaMP6f) between endogenous exons 1 and 2 of the *Gt(ROSA)26Sor* locus. *Ren1^c-GCaMP6f* mice are

generated by breeding *GCaMP6f*$^{fl/fl}$ with *Ren1*^{c}*-Cre* mice (*GCaMP6f*$^{fl/+}$*; Ren1*$^{c\text{-}cre/+}$). **B,** Immunofluorescence staining for renin (magenta) in the kidney cortex of the *Ren1*^{c}*-GCaMP6f* mice. Nuclei are stained with Hoechst (blue). The merged image shows GCaMP6f (green) expressed in the juxtaglomerular (JG) area around glomeruli stained with an anti-renin antibody. **C–D,** Time series of captured images (63 × magnification) of a kidney slice from *Ren1*^{c}*-GCaMP6f* mice with 3 nM angiotensin II (Ang II) stimulation. (**C**) White arrows point to the JG cells during intense GCaMP6f expression. (**D**) The orange dashed lines encircle the individual JG cells adjacent to each other. Individual JG cells can be distinguished by cytosolic GCaMP6f blinking periodically (see also Supplementary Movie 1). The time series starts when oscillatory Ca^{2+} waves fully develop. **E–F,** Time-series of fluorescent intensity at 0.1-second intervals (**E**) and the kymograph (**F**) of GCaMP6f-expressing JG cells with 3 nM Ang II stimulation (2 mM Ca^{2+}). The kymographs indicate changes in Ca^{2+} activity across designated reslice lines (black arrow) spanning adjacent JG cells. The activity of the GCaMP6f reporter visualizes oscillatory Ca^{2+} waves in distinct JG cells and the sequential Ca^{2+} activity between adjacent cells. All image dashed white circles indicate glomeruli. All image scale bar, 20 μm.

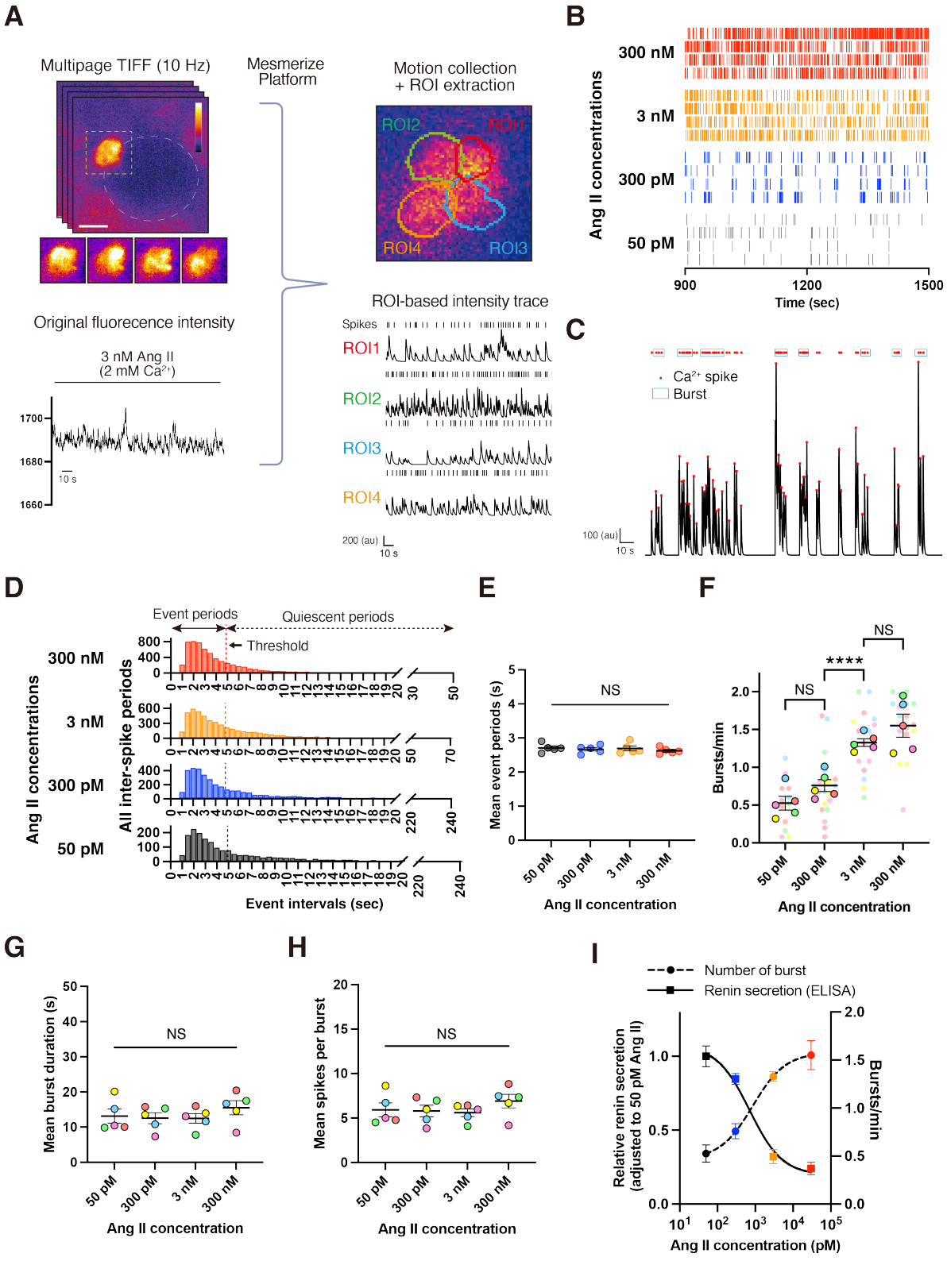

Figure 2. Structure of Ang II elicited Ca^{2+} spike patterns (bursts) and suppresses renin secretion within the JG cell cluster.

A, Schematic strategy for the region of interest (ROIs)-based fluorescence intensity trace of the spatiotemporal cropped JG cell cluster. The captured time series of JG cell cluster areas were cropped from multipage TIFF image sequences (10 Hz). A yellow dashed square line indicates a cropped JG area, shown below in representative images. The lower left plot indicates an example of consecutive fluorescence intensity of cropped JG cell clusters perfused by 3 nM Ang II solution suspended in 2 mM Ca^{2+} buffer and ROI-based fluorescence intensity trace. Mesmerize platform performs motion correction and ROI extraction from the imported fluorescence intensity of the spatiotemporal cropped JG cell cluster. Ca^{2+} transient spikes of each ROI are shown as raster plots corresponding to the intensity trace peaks. **B,** Representative raster plots for Ca^{2+} spikes in JG cell clusters imaged over 25 minutes under treatment with 50 pM, 300 pM, 3 nM, and 300 nM Ang II. The raster plots for the four ROIs captured in the last 10 minutes are shown. **C,** Example of trace data from JG cells treated with 3 nM Ang II and the successive Ca^{2+} spike and burst assignment. Ca^{2+} spikes (red dots) are grouped within a burst (blue squares) if the distance from the previous Ca^{2+} spike is less than the calculated threshold. A burst requires at least three consecutive spikes below the threshold to qualify. **D–H,** Analysis for Ca^{2+} spikes in JG cell clusters imaged over 25 minutes under treatment with 50 pM (N=4 mice and 5 slices, n=15 ROIs), 300 pM (N=5 mice and 5 slices, n=22 ROIs), 3 nM (N=5 mice and 5 slices, n=18, ROIs), and 300 nM Ang II (N=5 mice and 5 slices, n=17 ROIs). Histogram of all spike intervals across all ROIs in five JG cell clusters across Ang II concentrations are shown in (**D**). Thresholds are determined by the intersection of the Gaussian and exponential components of the distribution to divide event periods and quiescent periods (see also Supplementary Figure 3). The

mean event periods in a JG cell cluster (**E**) showed no notable variances across the groups (one-way ANOVA). The number of bursts/min (**F**) is dose-dependently increased, especially between 300 pM and 3 nM Ang II (a linear mixed model analysis with Tukey's multiple comparison test). The circle, which is the same color, represents ROIs analyzed from the same JG cell clusters. The mean burst duration (**G**) and mean spike per burst (**H**) showed no significant difference among the groups (one-way ANOVA). **I,** Fold increase in renin secretion in kidney slice preparations after stimulation with one of four Ang II concentrations (left y-axis, plotted relative to unstimulated secretion and adjusted to the value of 50 pM Ang II, n=4 for each concentration, non-linear regression fit: R^2=0.92, EC_{50}=707.1 pM), which is inversely correlated with the dose dependence of the number of bursts/min per slices (right y-axis, non-linear regression fit: R^2=0.81, EC_{50}=860.0 pM). Symbols are color-coded based on experimental conditions: 50 pM Ang II; black, 300 pM Ang II; blue, 3 nM Ang II; orange, and 1 μM Ang II; red. All data are shown as mean ± SEM. ****; P<0.0001, NS; no significance.

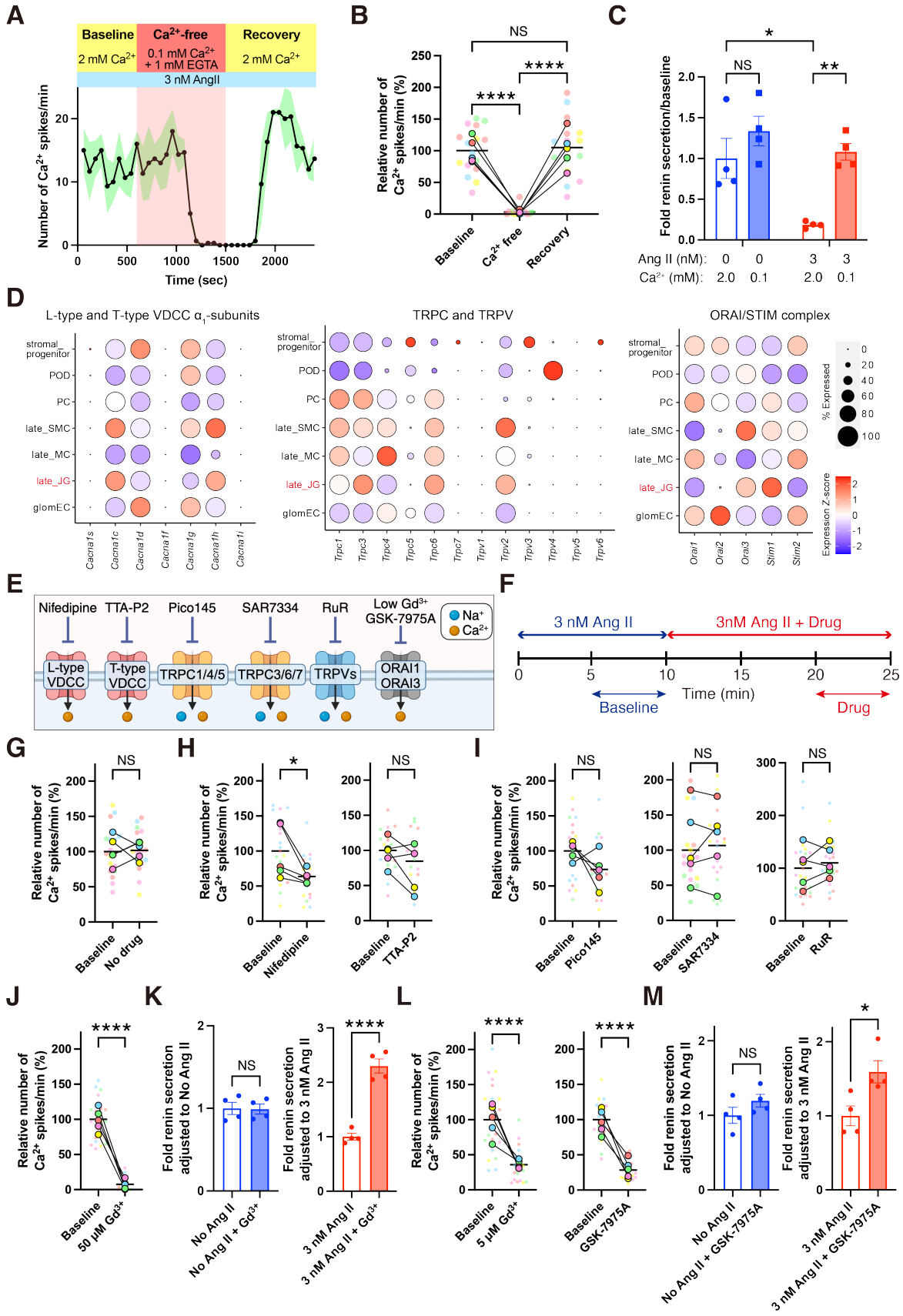

Figure 3. ORAI channels mainly mediate Ang II-elicited Ca^{2+}-oscillations and renin secretion in JG cells among the cell membrane Ca^{2+} permeable channels.

A, A representative time course of the number of Ca^{2+} spikes/min in each ROI (n=3 ROIs). The kidney slice was stimulated with 2 mM Ca^{2+} buffer (Baseline) for 10 min, 0.1 mM Ca^{2+} + 1 mM EGTA buffer (Ca^{2+}-free) for 15 min, and 2 mM Ca^{2+} buffer again (Recovery) for 15 min. The time course of green-shaded areas represents SEM. **B,** A summarized data showing the effect of transiently removing and washing back extracellular Ca^{2+} on JG cells. The percentage of spikes/minute of JG cells in Baseline, Ca^{2+}-free, and Recovery at last 5 min following exposure to a solution are shown (adjusted to Baseline, N=4 mice and 5 slices, n=16 ROIs, a linear mixed model analysis with Tukey's multiple comparison test). The circle, which is the same color, represents JG cells analyzed from the same kidney slice. **C,** Fold increase in renin secretion in kidney slice preparations after incubation with 2 mM Ca^{2+} PIPES buffer and Ca^{2+}-free buffer (0.1 mM Ca^{2+} + 1 mM EGTA) under No-Ang II and 3 nM Ang II, plotted relative to unstimulated secretion and adjusted to the value of No-Ang II in 2 mM Ca^{2+} PIPES buffer (n=4 for each concentration, two-way ANOVA; Šídák's multiple comparison test). All data are shown in mean ± SEM. **D.** Bubble plots showing gene expression profiles of L- and T-type voltage-dependent Ca^{2+} channels (VDCC) α_1-subunits, Canonical TRP (TRPC) and vanilloid TRP (TRPV) subfamilies, and ORAI/STIM complex in the renin lineage cell-related clusters using single-cell RNA-seq data of *FoxD1*$^{+}$ progenitor cells isolated from *FoxD1*$^{cre/+}$*; R26R-mTmG* mice kidney at postnatal day 30 (P30). POD; podocyte, PC, pericyte, late_SMC; smooth muscle cell in P30, late_MC; mesangial cell in P30, late_JG; juxtaglomerular cell in P30, glomEC; glomerular endothelial cell. **E–F,** Schematic for pharmacological ion channel inhibition screening for JG cells by *ex vivo* Ca^{2+} imaging using *Ren1*^{c}*-GCaMP6f* mouse kidney. Our target

channels and inhibitors are illustrated in (**E**). The pharmacological screening timeline is shown in (**F**). After a 10-minute baseline acquisition period, slices were perfused with a buffer containing a vehicle or drug and imaged for 15 minutes. The average number of Ca^{2+} spikes/min of the first and last 5 minutes were examined to evaluate the effect of each application. **G–I,** The relative number of Ca^{2+} spikes/min (%) in captured JG cells adjusted to baseline. Application of 3 nM Ang II without inhibitors (no-inhibitor, the same experiments as Figure 2) is shown in (**G**). Blockades for voltage-dependent Ca^{2+} channels (VDCC) are shown in (**H**). 10 μM nifedipine is applied for blocking pan L-type VDCC (N=4 mice and 5 slices, n=18 ROIs) and 10 μM TTA-P2 for T-type VDCC (N=5 mice and 5 slices, n=18 ROIs). Blockades for Canonical TRP (TRPC) and vanilloid TRP (TRPV) subfamilies are shown in (**I**). 10 μM Pico145 is applied for blocking the TRPC1/4/5 subfamily (N=5 mice and 5 slices, n=17 ROIs), 10 μM SAR7334 for the TRPC3/6/7 subfamily (N=4 mice and 5 slices, n=20 ROIs), and 10 μM Ruthenium red (RuR) for pan TRPV, respectively (N=4 mice and 5 slices and 5 mice each, n=25 ROIs). **J**, The relative number of Ca^{2+} spikes/min (%) in captured JG cells treated with 50 μM Gd^{3+} (N=4 mice and 5 slices each, n=23 ROIs). **L,** Fold increase in renin secretion in kidney slice preparations 30 minutes after treatment with and without 50 μM Gd^{3+} under 3 nM and no Ang II (plotted relative to unstimulated secretion and adjusted to the value of no treatment, N=4 for each concentration, Student's two-tailed t-test). **K,** The relative number of Ca^{2+} spikes/min (%) in JG cells by blocking ORAI channels with 5 μM Gd^{3+} (N=4 mice and 5 slices, n=22 ROIs) and 10 μM GSK-7975A (N=4 mice and 5 slices, n=20 ROIs). **M**, Fold increase in renin secretion in kidney slice preparations 30 minutes after treatment with and without 10 μM GSK-7975A under 3 nM and no Ang II (plotted relative to unstimulated secretion and adjusted to the value of no treatment, N=4 for each concentration, Student's two-tailed t-test). All data are shown as mean ± SEM. A linear

mixed model analysis calculates P-values in **G**, **H**, **I**, **J**, and **L**. The circle, which is the same color, represents ROIs analyzed from the same kidney slice. *; P<0.05, **; P<0.01, ****; P<0.0001, NS; no significance.

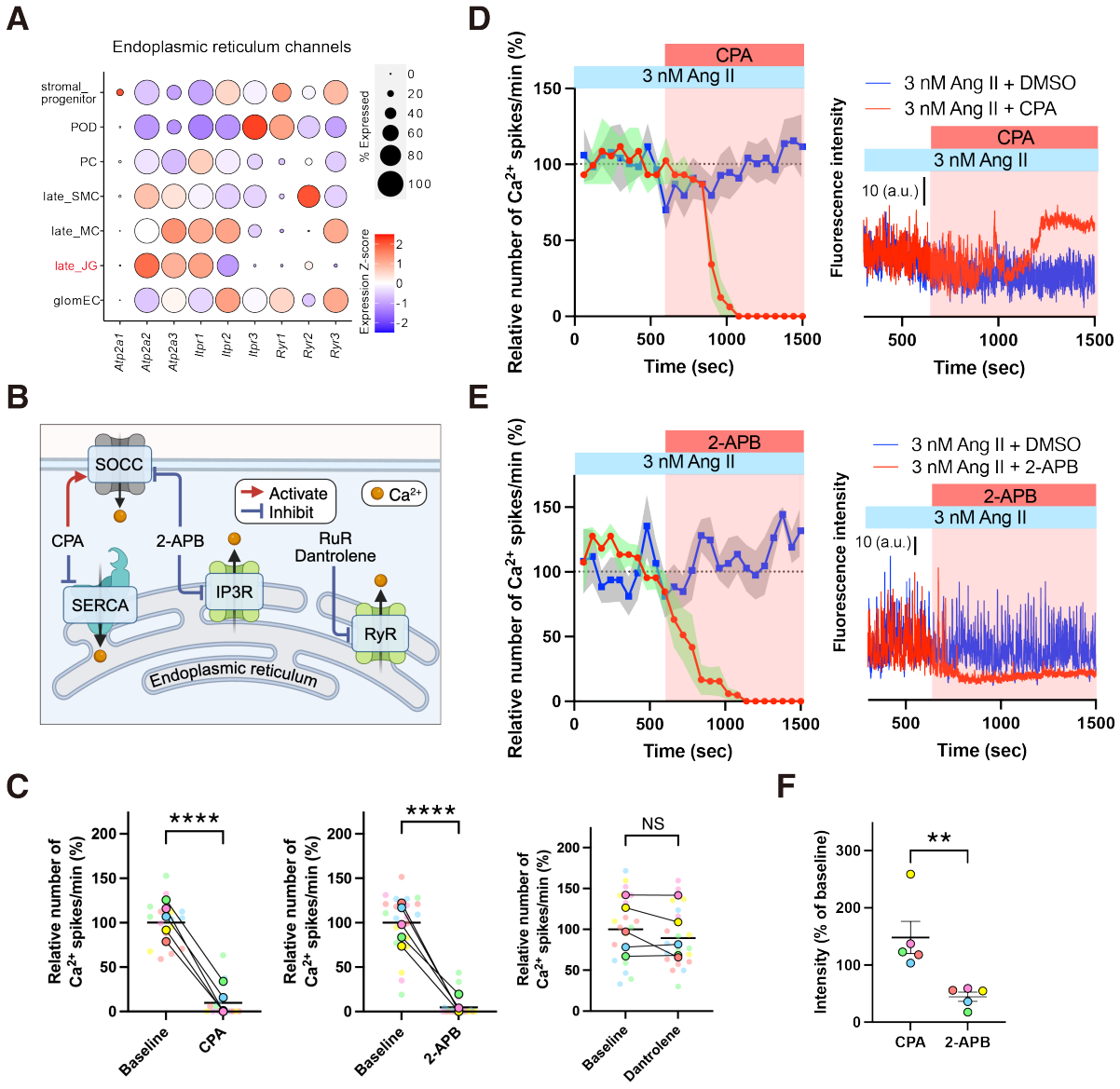

Figure 4. Endoplasmic reticulum Ca^{2+} stores and releases generate Ca^{2+} oscillatory signals induced by Ang II in JG cells.

A, Bubble plots showing gene expression profiles of endoplasmic reticulum (ER) channels in the renin lineage cell-related clusters using single-cell RNA-seq data of *FoxD1*$^{+}$ progenitor cells isolated from *FoxD1*$^{cre/+}$*; R26R-mTmG* mice kidney at postnatal day 30 (P30). POD; podocyte, PC, pericyte, late_SMC; smooth muscle cell in P30, late_MC; mesangial cell in P30, late_JG;

juxtaglomerular cell in P30, glomEC; glomerular endothelial cell. **B,** Schematic for pharmacological ER channel inhibition and the inhibitors. CPA was used to block sarcoplasmic/endoplasmic reticulum Ca^{2+}-ATPase (SERCA) while activating the store-operated Ca^{2+} (SOC) channel. 2-Aminoethoxydiphenyl borate (2-APB) was used to block an inositol trisphosphate receptor (IP3R). 100 μM 2-APB also inhibits SOCC. Dantrolene was used to block a ryanodine receptor (RyR). Ruthenium red (RuR), used as a pan TRPV inhibitor (Figure 3I), also inhibits RyR. **C,** The relative number of Ca^{2+} spikes/min (%) under 3 nM Ang II treatment with 20 μM CPA (N=4 mice and 5 slices, n=16 ROIs), 100 μM 2-APB (N=5 mice and 5 slices, n=21 ROIs), and 10 μM Dantrolene (N=5 mice and 5 slices, n=20 ROIs), respectively. The strategy is the same as Figure 3F. The circle, which is the same color, represents JG cells analyzed from the same kidney slice. A linear mixed model analysis calculates P-values. All data are shown as mean ± SEM. **D–E,** Representative time courses of the number of Ca^{2+} spikes (left) and original fluorescence intensities of cytosolic GCaMP6f (right) before and after perfusion of CPA (**D**, n=2 ROIs) or 2-APB (**E**, n=4 ROIs) under 3 nM Ang II treatment. The data for treatment with the same volume of DMSO (n=4, 5 ROIs, respectively) are shown as controls. The time course of green- and gray-shaded areas represents SEM. **F,** The percentage of fluorescence intensities treated with CPA and 2-APB compared to the baselines. Mann-Whitney U test calculates the P-value. **; P<0.01, ****; P<0.0001, NS; no significance.

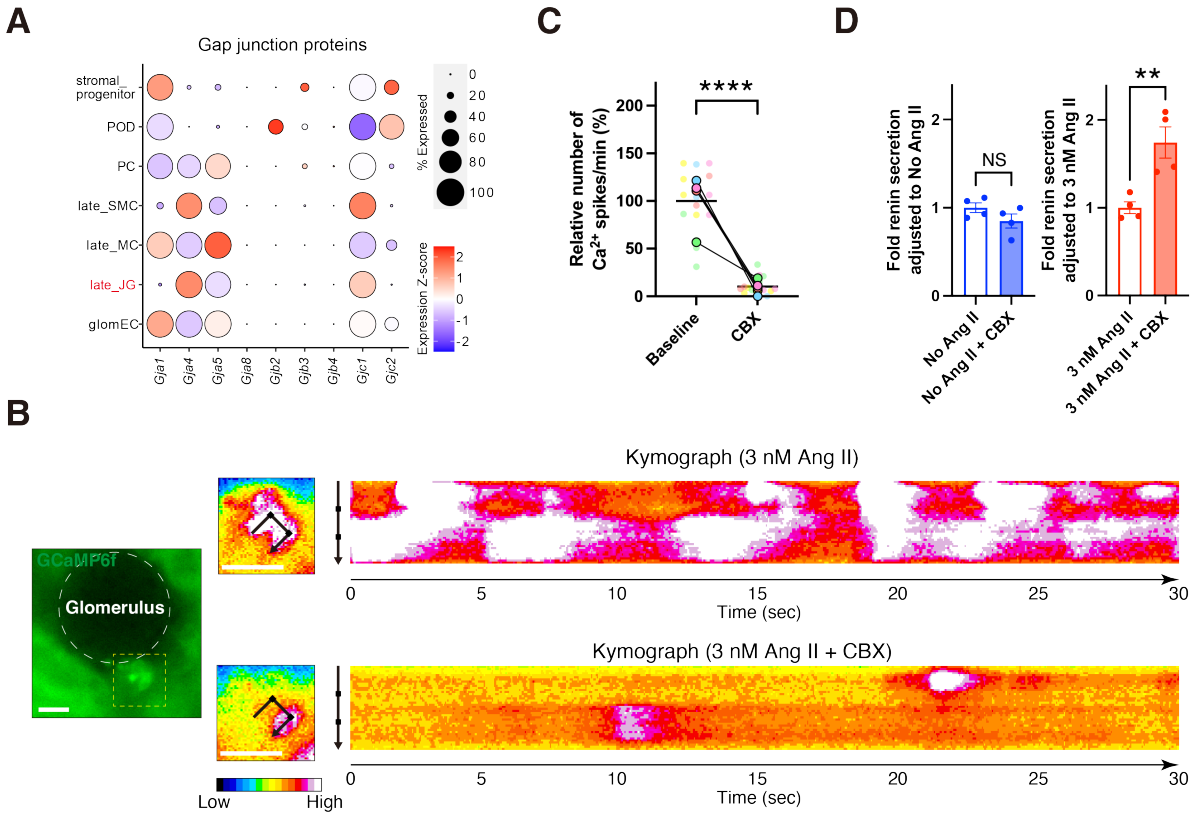

Figure 5. Gap junction inhibition blocks intra- and inter-cellular Ca^{2+} activity within the JG cell cluster.

A, Bubble plots showing gene expression profiles of gap junction proteins in the renin lineage cell-related clusters using single-cell RNA-seq data of *FoxD1*$^{+}$ progenitor cells isolated from *FoxD1*$^{cre/+}$*; R26R-mTmG* mice kidney at postnatal day 30. *Gja1*; Conneixin43 (Cx43), *Gja4*; Cx37, *Gja5*; Cx40, *Gja8*; Cx50, *Gjb2*; Cx26, *Gjb3*; Cx31, *Gjb4*; Cx30.3, *Gjb5*; Cx31.1, *Gjc1*; Cx45, *Gjc2*; Cx47. **B,** Representative kymographs show the time series of fluorescent intensity under 3 nM Ang II (top) and 3 nM Ang II + 100 μM carbenoxolone (CBX) perfusion (bottom). See also Supplementary Movie 2. **C**, The relative number of Ca^{2+} spikes/min (%) in captured JG cells treated with 100 μM CBX (N=4 mice and 5 slices each, n=16 ROIs, A linear mixed model analysis calculates the P-value). **D,** Fold increase in renin secretion in kidney slice preparations

30 minutes after treatment with and without 100 μM CBX under 3 nM and no Ang II (plotted relative to unstimulated secretion and adjusted to the value of no treatment, N=4 for each concentration, Student's two-tailed t-test). All data are shown as mean ± SEM. The circle, which is the same color, represents JG cells analyzed from the same kidney slice. **; P<0.01, ****; P<0.0001, NS; no significance.

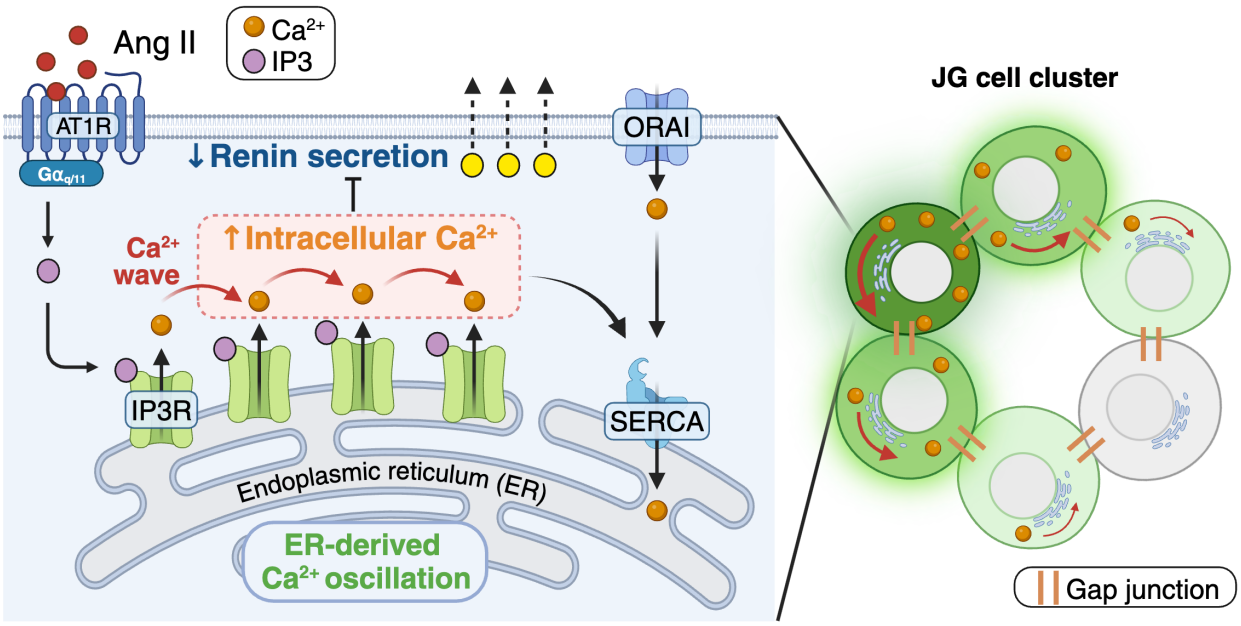

Figure 6. Overview of Ang II-elicited inter- and intra-Ca^{2+} dynamics within the JG cell cluster.

Ang II dosed-dependently induces robust and sustained Ca^{2+}-oscillations within their native JG cell cluster and suppresses renin secretion. These coordinated Ca^{2+} signaling are mediated by intracellular Ca^{2+} release at the endoplasmic reticulum supplied through ORAI channels and inter-cellular gap junctions that propagate signaling molecules. Ang II; angiotensin II, AT1R; angiotensin II receptor type 1; ER; endoplasmic reticulum, IP3R; 1,4,5-trisphosphate (IP3) receptor, JG; juxtaglomerular, SERCA; sarcoplasmic/endoplasmic reticulum Ca^{2+}-ATPase.

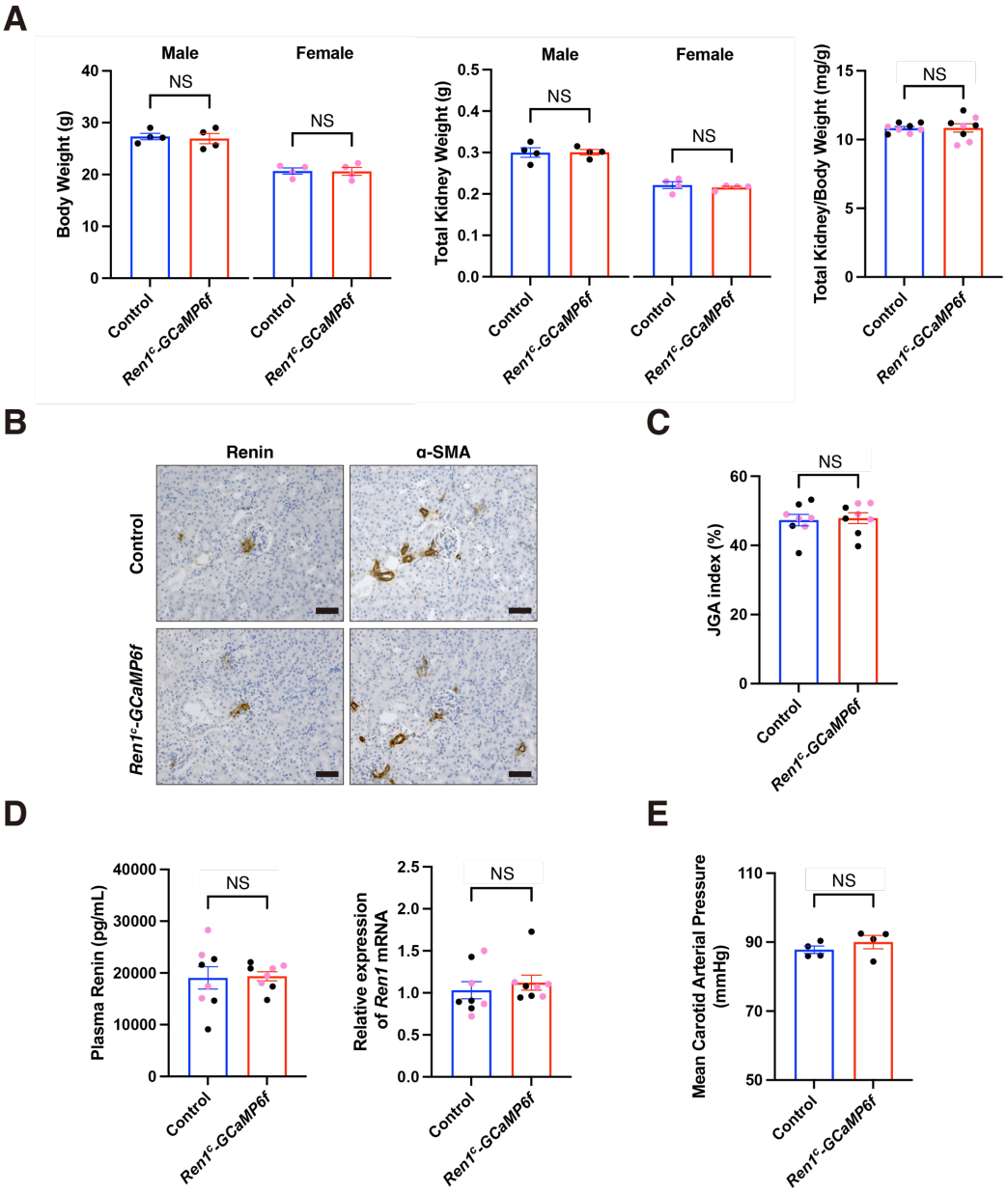

Supplementary Figure 1, *Ren1*^{c}*-GCaMP6f* mice show normal kidney development and renin expression in juxtaglomerular cells. A, Body weight and total kidney weight showed no significant difference between *Ren1*^{c}*-GCaMP6f* mice (79–81 days old, n=4 for males and n=4 for females) and Control (81 days old of C57BL/6 mice, n=4 for males and n=4 for females) in both males and females (Student's two-tailed t-test). The Total kidney/body weight ratio also showed no significant difference between *Ren1*^{c}*-GCaMP6f* mice and Control (Student's two-tailed t-test).

B, Immunohistochemistry for renin and α-smooth muscle actin (α-SMA) on the consecutive sections showed no abnormality of the kidneys from *Ren1^{c}-GCaMP6f* mice. Scale bar, 50 μm **C,** Juxtaglomerular apparatus (JGA) index showed no significant difference between *Ren1^{c}-GCaMP6f* mice (Student's two-tailed t-test). **D,** Plasma renin concentration (left) and *Ren1* mRNA in the kidney cortices (right) from *Ren1^{c}-GCaMP6f* mice at normal states did not show significant differences compared to the Controls (Student's two-tailed t-test). All data are reported as means ± SEM. Black dots show male samples and purple dots show female samples. **E,** Mean carotid arterial pressure showed no significant difference between *Ren1^{c}-GCaMP6f* mice (n=4, Student's two-tailed t-test). NS; no significance.

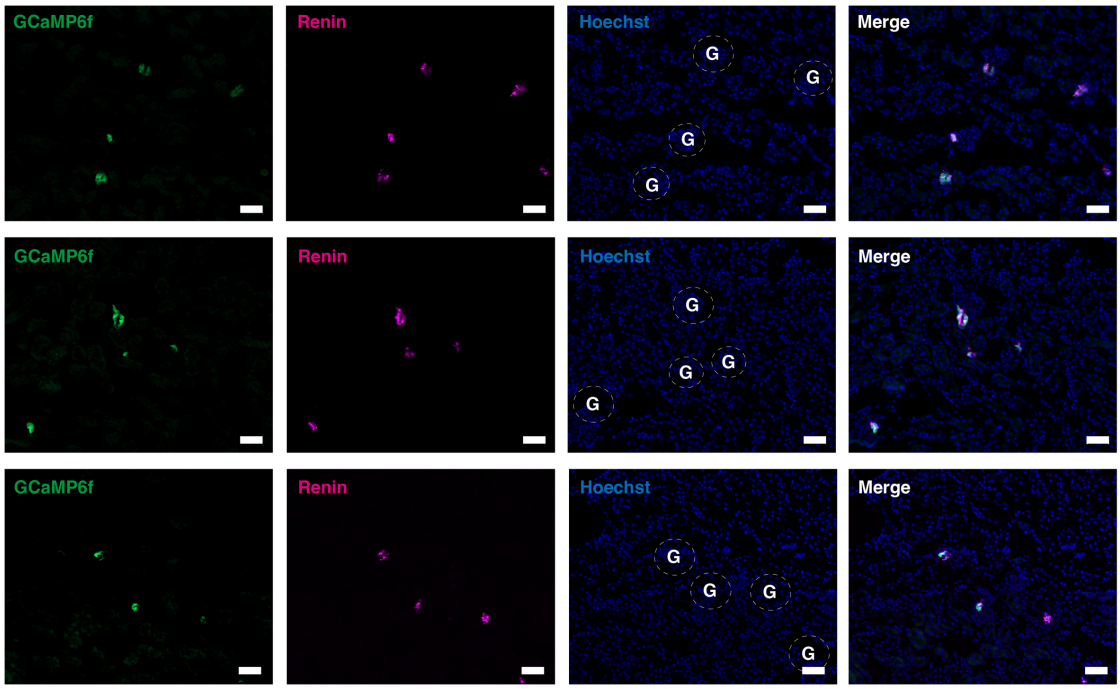

Supplementary Figure 2, Colocalization of GCaMP6f and renin around the juxtaglomerular area of *Ren1^{c}-GCaMP6f* mouse kidney. Immunofluorescence staining for renin (magenta) in the kidney cortex of the *Ren1^{c}-GCaMP6f* mice. Nuclei are stained with Hoechst (blue). The merged image shows GCaMP6f (green) expressed in the juxtaglomerular area around glomeruli stained with an anti-renin antibody. Dashed white circles indicate glomeruli. G; Glomerulus. Scale bar, 50 μm.

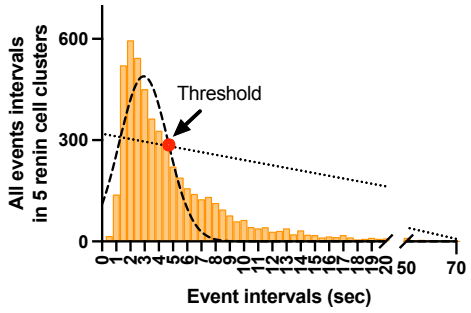

Ang II concentrations	The intersection of Gaussian and Exponential
50 pM	4.969357
300 pM	4.81473
3 nM	4.813218
300 nM	4.827458

Supplementary Figure 3, Calculations for determining threshold values for defining event periods. The histogram of all inter-spike periods across all ROIs in five JG cell clusters treated with 3 nM Ang II is shown. The solid line indicates the Gaussian curve, and the dotted line indicates the exponential components. The intersection of the Gaussian and exponential components (red dot) is used for the Gaussian-exponential model (thresholds). The table shows thresholds for the maximum intra-burst interval as calculated from the Gaussian-exponential model for each Ang II dose (50 pM, 300 pM, 3 nM, and 300 nM).

Supplementary Movie 1. Angiotensin II elicits robust oscillatory Ca^{2+} signals coordinated within the juxtaglomerular cell cluster.

Time series of captured juxtaglomerular cell images at the juxtaglomerular area in a kidney slice from *Ren1^{c}-GCaMP6f* mice under 3 nM angiotensin II containing 2 mM Ca^{2+} buffer perfusion. Yellow arrows point to the juxtaglomerular cells during intense GCaMP6f expression. Scale bar, 20 μm.

Supplementary Movie 2. A pan gap junction inhibitor suppresses Ang II-elicited Ca^{2+} oscillations within the juxtaglomerular cell cluster.

Time series of captured juxtaglomerular cell images at the juxtaglomerular area in a kidney slice from *Ren1^{c}-GCaMP6f* mice under 3 nM angiotensin II with (left) and without (right) 100 μM carbenoxolone treatment. Yellow arrows point to the juxtaglomerular cells during intense GCaMP6f expression Scale bar, 20 μm.

Data are provided separately.